

2012

Microwave Remote Sensing of Soil Moisture Science and Applications

Son V. Nghiem
California Institute of Technology

Brian D. Wardlow
University of Nebraska - Lincoln, bwardlow2@unl.edu


David Allured
National Oceanic and Atmospheric Administration

Mark Svoboda
University of Nebraska - Lincoln, msvoboda2@unl.edu

Doug LeComte
National Oceanic and Atmospheric Administration

See next page for additional authors

Follow this and additional works at: <http://digitalcommons.unl.edu/droughtfacpub>

 Part of the [Climate Commons](#), [Environmental Indicators and Impact Assessment Commons](#), [Environmental Monitoring Commons](#), [Hydrology Commons](#), [Other Earth Sciences Commons](#), and the [Water Resource Management Commons](#)

Nghiem, Son V.; Wardlow, Brian D.; Allured, David; Svoboda, Mark; LeComte, Doug; Rosencrans, Matthew; Chan, Steven K.; and Neumann, Gregory, "Microwave Remote Sensing of Soil Moisture Science and Applications" (2012). *Drought Mitigation Center Faculty Publications*. 104.

<http://digitalcommons.unl.edu/droughtfacpub/104>

This Article is brought to you for free and open access by the Drought -- National Drought Mitigation Center at DigitalCommons@University of Nebraska - Lincoln. It has been accepted for inclusion in Drought Mitigation Center Faculty Publications by an authorized administrator of DigitalCommons@University of Nebraska - Lincoln.

Authors

Son V. Nghiem, Brian D. Wardlow, David Allured, Mark Svoboda, Doug LeComte, Matthew Rosencrans, Steven K. Chan, and Gregory Neumann

Published in *Remote Sensing of Drought: Innovative Monitoring Approaches*, edited by Brian D. Wardlow, Martha C. Anderson, & James P. Verdin (CRC Press/Taylor & Francis, 2012).

This chapter is a U.S. government work and is not subject to copyright in the United States.

Authors:

Son V. Nghiem

Jet Propulsion Laboratory
California Institute of Technology
Pasadena, California

Brian D. Wardlow

National Drought Mitigation Center
School of Natural Resources
University of Nebraska–Lincoln
Lincoln, Nebraska

David Allured

Physical Science Division
Earth System Research Laboratory
National Oceanic and Atmospheric Administration
Boulder, Colorado

Mark D. Svoboda

National Drought Mitigation Center
School of Natural Resources
University of Nebraska–Lincoln
Lincoln, Nebraska

Doug LeComte

Climate Prediction Center
National Oceanic and Atmospheric Administration
Camp Springs, Maryland

Matthew Rosencrans

Climate Prediction Center
National Oceanic and Atmospheric Administration
Camp Springs, Maryland

Steven K. Chan

Jet Propulsion Laboratory
California Institute of Technology
Pasadena, California

Gregory Neumann

Jet Propulsion Laboratory
California Institute of Technology
Pasadena, California

9 Microwave Remote Sensing of Soil Moisture

Science and Applications

*Son V. Nghiem, Brian D. Wardlow,
David Allured, Mark D. Svoboda,
Doug LeComte, Matthew Rosencrans,
Steven K. Chan, and Gregory Neumann*

CONTENTS

9.1	Introduction	197
9.2	Microwave Remote Sensing Science	198
9.2.1	Passive Remote Sensing.....	199
9.2.2	Active Remote Sensing.....	200
9.2.3	Passive and Active Blending.....	202
9.3	Drought Applications.....	206
9.3.1	Drought Monitoring Issues	206
9.3.2	Uses of Satellite Data.....	206
9.3.2.1	Temporal Data at Local Scale.....	206
9.3.2.2	Spatial Data at Regional Scale.....	207
9.3.2.3	Spatial Data at Continental Scale	210
9.3.2.4	Soil Moisture Products for Drought Monitoring and Forecasting	213
9.4	Summary and Concluding Remarks.....	219
	Acknowledgments.....	222
	References.....	222

9.1 INTRODUCTION

Soil moisture is a fundamental link between global water and carbon cycles and has major applications in predicting natural hazards such as droughts and floods (National Research Council, 2007). From precipitation data, soil wetness can be estimated by hydrological land-surface models. In the United States, preliminary precipitation data are based on measurements gathered from many active stations nationwide each month, and it takes 3–4 months to assemble final, quality-controlled data. In the western United States, some climate divisions may have no stations reporting in a particular month or may lack first- or second-order stations, and

significant blockages by mountains limit the capability of precipitation measurement by surface rain radars (Maddox et al., 2002).

Soil moisture can also be measured directly, using data from networks like the Oklahoma Mesonet System (Illston et al., 2004) and the Soil Climate Analysis Network (SCAN) (USDA, 2009a). However, measurements from such networks are generally too sparse for most applications and are of varying accuracy. Soil moisture observations have been added to the SNOTEL network (USDA, 2009b), but fully calibrated data are not yet available routinely. Given the limited number of stations collecting point-based, in situ data, this information may not be representative of regional soil moisture conditions.

Soil moisture measurements over a large spatial extent (areal data rather than point data) with few or no missing gaps are crucial for characterizing the land surface water distribution from regional to continental scales. Recognizing the importance of soil moisture as a key variable for drought monitoring, satellite microwave remote sensing soil moisture retrievals using both passive and active sensors hold the potential to begin to fill this informational void in the United States and elsewhere.

Passive microwave radiometers, such as the Scanning Multichannel Microwave Radiometer (SMMR), Special Sensor Microwave/Imager (SSM/I), Tropical Rainfall Measuring Mission (TRMM) Microwave Imager (TMI), Advanced Microwave Scanning Radiometer on the Earth Observing System (AMSR-E), and Soil Moisture and Ocean Salinity sensor (SMOS), measure the natural emission of microwave energy from the land surface, which is used to derive soil moisture using various algorithms (Wang, 1985; Owe et al., 1988; Kerr and Njoku, 1990; Teng et al., 1993; van de Griend and Owe, 1994; Engman, 1995; Jackson, 1997; Kerr et al., 2001; Njoku et al., 2003). These passive radiometers operate at microwave frequencies from L to Ka bands with additional higher frequencies for other applications.

In contrast, active sensors, including synthetic aperture radar (SAR) and scatterometers, transmit signals to a targeted surface area and measure the scattering return. Many approaches have been used to estimate soil moisture from data sets acquired by SARs including Seasat, Spaceborne Imaging Radar-C (SIR-C), European Remote Sensing (ERS), RADARSAT, Environmental Satellite (Envisat), and Advanced Land Observing Satellite (ALOS) (Blanchard and Chang, 1983; Cognard et al., 1995; Dubois et al., 1995; Loew et al., 2006; Shrivastava et al., 2009; Takada et al., 2009), and by scatterometers such as ERS and QuikSCAT (QSCAT) (Wagner et al., 1999; Nghiem et al., 2000; Wagner and Scipal, 2000). In this chapter, we review the science principle of active and passive remote sensing of soil moisture and then illustrate results from AMSR-E and QSCAT for drought applications.

9.2 MICROWAVE REMOTE SENSING SCIENCE

The principle of microwave remote sensing of soil moisture is based on the sensitivity of soil permittivity to the amount of liquid water. The permittivity of a medium, like moist soil, characterizes electromagnetic wave propagation and attenuation in the medium. Both brightness temperature (BT) (measured by a radiometer) and backscatter (measured by a radar) are dependent on the soil permittivity. Empirical models have been developed in order to relate volumetric content (m_v) for different soil types to the

dielectric constant (the permittivity of a medium relative to that of free space) at microwave frequencies between 1.4 and 18 GHz (Dobson et al., 1985; Hallikainen et al., 1985).

Although in situ measurements of soil dielectric constant can be made with a probe (Jackson, 1990), satellite remote sensors do not directly provide soil dielectric measurements. Instead, these sensors acquire BT or backscatter signatures, which are dependent on soil dielectric properties and thus soil moisture. Such a relationship enables the inversion of soil moisture from BT or backscatter data, but it can be complicated by vegetation cover, surface roughness, rainfall, and anthropogenic effects (e.g., radio frequency interference [RFI]), which have different impacts on the accuracy of soil moisture retrieval at different microwave frequencies.

9.2.1 PASSIVE REMOTE SENSING

The retrieval of soil moisture from BT has been studied by many researchers (see summary by Njoku et al., 2003) and is reviewed briefly here. For an isothermal vegetated soil surface with physical temperature T_s , BT (T_{bp}) can be expressed as follows:

$$T_{bp} = T_s \left\{ e_{sp} \exp(-\tau_c) + (1 - \omega_p) [1 - \exp(-\tau_c)] [1 + r_{sp} \exp(-\tau_c)] \right\} \quad (9.1)$$

where the soil emissivity is $e_{sp} = 1 - r_{sp}$ for soil reflectivity r_{sp} , which is influenced by soil moisture through the effect of moisture on the soil dielectric constant. In Equation 9.1, τ_c and ω_p are the vegetation opacity and the vegetation single scattering albedo, respectively. Multiple scattering in the vegetation layer is neglected, and a quasi-specular soil surface and no reflection at the air-vegetation boundary are assumed in Equation 9.1. Vegetation opacity and multiple scattering have less effect at lower microwave frequencies. The effective emitting depth is controlled by the near-surface moisture profile and is smaller for higher microwave frequencies and for wetter soils. Although microwaves can only sense soil moisture in the top soil layer (in millimeters to decimeters, depending on frequencies), there is a correlation to soil moisture in deeper soil at night when the soil moisture and temperature profiles are more uniform.

For a fixed viewing angle, an empirical formulation has been found useful for relating the reflectivity of a rough soil surface, r_{sp} , to that of the equivalent smooth surface, r_{oq} (Wang and Choudhury, 1981; Wang, 1983), which is expressed as follows:

$$r_{sp} = [(1 - Q)r_{op} + Qr_{oq}] \exp(-h) \quad (9.2)$$

where

p and q represent either of the orthogonal polarization states (vertical, v, or horizontal, h)

Q and h are roughness parameters

Q may be approximated as zero at low frequencies (e.g., L and C bands). The separation of soil moisture and roughness effects through Equation 9.2 is not precise, and the parameter h has a residual moisture dependence (Li et al., 2000; Wigneron et al., 2001).

To normalize the surface temperature (T_s) dependence in Equation 9.1, the polarization ratio (PR) is obtained by

$$PR = \frac{T_{bv} - T_{bh}}{T_{bv} + T_{bh}} \quad (9.3)$$

which is suitable for multichannel data taken at the same incidence angle (Kerr and Njoku, 1990). At large incidence angles (e.g., $>50^\circ$), the difference between the vertically and horizontally polarized BTs for bare soils is large, giving rise to a significant PR signal. However, the observation path length through the vegetation becomes longer at large incidence angles, increasing vegetation attenuation and thus decreasing sensitivity to soil moisture.

While Equations 9.1 through 9.3 form a general theoretical basis for soil moisture retrieval from passive microwave data, several approaches have been developed for different satellite data sets using different methods to correct for effects of soil type, roughness, vegetation, and surface temperature (Njoku et al., 2003). Nevertheless, further advances are needed for various nonisothermal conditions and multiple interactions between the soil surface and vegetation cover at different growth stages. For data from the AMSR-E on the EOS Aqua satellite, the soil moisture retrieval utilizes primarily the frequency channels of 10.7 and 18.7 GHz to consider effects of atmospheric and vegetative attenuation and to minimize the requirement for ancillary data inputs. The TMI has 10.7 and 19.3 GHz channels, which can be used to obtain PR for soil moisture applications with a better consistency at the lower frequency (Njoku et al., 2003). Further details of the retrieval can be found in the literature (Njoku and Li, 1999; Njoku et al., 2003; Njoku, 2004).

9.2.2 ACTIVE REMOTE SENSING

In active remote sensing, soil moisture can be derived from backscatter measured by an SAR at a high spatial resolution with a limited spatial and infrequent repeat coverage and by a scatterometer at a low spatial resolution with a large areal and frequent coverage. Many theoretical models have been developed to characterize backscatter signatures of vegetated soil. Here, a scattering model based on the analytic vector wave theory (Nghiem et al., 1993a) together with a practical formulation is reviewed.

Backscatter σ_0 from moist soil with vegetation cover is determined from an ensemble average of the correlation of scattered field components E as follows:

$$\begin{aligned} \langle \bar{E}_{0s}(\bar{r}) \cdot \bar{E}_{0s}^*(\bar{r}) \rangle &= \sum_{i,j,k,l,m}^{x,y,z} k_0^4 \int_0^\pi d\psi_f \int_0^{2\pi} d\phi_f p(\psi_f, \phi_f) \int_{V_1} d\bar{r}_1 \int_{V_1} d\bar{r}_1^0 C_{\xi 1jklm}(\bar{r}, \bar{r}_1^0; \psi_f, \phi_f) \\ &\times \left[\langle G_{01ij}(\bar{r}, \bar{r}_1) \rangle \langle F_{1k}(\bar{r}_1) \rangle \right] \cdot \left[\langle G_{01il}(\bar{r}, \bar{r}_1^0) \rangle \langle F_{1m}(\bar{r}_1^0) \rangle \right]^* \quad (9.4) \end{aligned}$$

where subscript 0 represents the air space above the vegetation, and subscript 1 indicates the vegetation cover occupying volume V_1 over the soil surface. The dyadic Green's function G and the mean field F are obtained as described by Nghiem et al. (1990). The correlation function C characterizes the vegetation scatterers having different size, shape, and orientation angle ψ_f in elevation and ϕ_f in azimuth. For the vegetation canopy, the effective permittivity is calculated under the strong permittivity fluctuation theory, which accounts for wave attenuation including scattering and absorption loss (Nghiem et al., 1993a). The analytic vector wave theory accounts for fully polarimetric scattering, preserves the phase information, and includes multiple reflection and transmission interactions of upgoing and downgoing electromagnetic waves with the soil surface. The solution conveys soil moisture information, because soil transmissivity and reflectivity are controlled by the soil dielectric constant as a function of volumetric soil moisture.

Rough surface scattering can be included in the contribution to the total backscatter. The small-scale roughness of the soil surface is described with a standard deviation height and a slope. When a large-scale roughness also exists, the overall roughness is accounted for by a joint probability density function for both roughness scales (Nghiem et al., 1995). The vegetation volume scattering and soil surface scattering are assumed to be uncorrelated because of independent statistical representations of vegetation scatterers (e.g., leaves, twigs, and branches) and soil surface roughness. As a result, the total backscatter is a sum of the vegetation volume backscatter and soil surface backscatter. In the layer scattering configuration, such as a vegetation layer over a rough soil surface, contributions from the rough surface scattering are considered with wave interactions, differential propagation delay, and wave attenuation in the vegetation layer (Nghiem et al., 1995), which can be effectively anisotropic when vegetation scatters have a preferential directional structure (e.g., planophile, plagio-phile, erectophile, or extremophile orientation distribution) (Nghiem et al., 1993b).

The backscatter from a rough soil surface depends strongly on the soil dielectric constant and the transmissivity and reflectivity because of wave interactions with the soil boundary. Thus, the surface scattering also contains a soil moisture signature in addition to the soil moisture information in the interactive volume scattering components. However, a dense vegetation canopy can have a large imaginary part in its effective permittivity, which attenuates both the soil surface scattering and soil interactions in the volume scattering, and consequently masks the soil moisture signature. Specific mathematical details of the volume and surface scattering in layered media can be found in earlier publications by Nghiem et al. (1990, 1993a,b, 1995).

Although the formulation mentioned earlier provides physical insights and a theoretical basis for active remote sensing of soil moisture, in practice, it is not possible to set up a soil moisture inversion method strictly based on theoretical modeling of electromagnetic scattering because of the complexities of natural environments in different climate regimes. The alternative is a simple empirical linear equation that relates backscatter σ_0 to volumetric soil moisture m_v , as

$$\sigma_0 = am_v + b \quad (9.5)$$

where coefficients a and b are dependent on incidence angle, polarization, vegetation conditions, soil type, surface variation, and climate regime (Mo et al., 1984; Prevot et al., 1993; Shrivastava et al., 1997; Shoshany et al., 2000; Hutchinson, 2003). Particularly for Ku-band backscatter data from the SeaWinds scatterometer aboard the QSCAT satellite, the bias term b in Equation 9.5 contains a signature of seasonal vegetation change, while changes in volumetric soil moisture m_v from rainwater are detectable in backscatter variations in a timescale consistent with the initial impulse increase in wetness from the precipitation input throughout the subsequent drying process (Nghiem et al., 2005). Thus, soil moisture change (SMC) can be directly inferred from Equation 9.5 using the temporal backscatter-change method, which removes most of the background bias.

9.2.3 PASSIVE AND ACTIVE BLENDING

As presented in Sections 9.2.1 and 9.2.2, passive and active sensors measure different parameters: passive BT and active radar backscatter, each of which has different sensitivities to soil moisture and vegetation cover. This section explains how blending of passive and active can better represent the overall state of soil moisture on land surface compared to the separate use of each data type.

In the ideal theoretical case of smooth bare soil ($\tau_c = 0$), Equation 9.1 dictates that the BT is directly proportional to the emissivity e_{sp} , which is determined by soil dielectric constant and is thereby most sensitive to soil moisture. In comparison, there is no active radar backscatter because there is no vegetation ($V_1 = 0$ in Equation 9.4 without vegetation) and no rough surface; hence, the soil moisture is not measurable by a radar for bare soil without any roughness. For real surfaces, surface roughness and/or vegetation cover will exist and will affect the sensitivity to soil moisture differently in passive (Njoku et al., 2003) versus active data (Nghiem et al., 1993a) until the vegetation cover becomes sufficiently dense to start masking the soil effects.

As an illustration of passive and active blending, a correlation analysis was conducted comparing satellite-based remote sensing signatures to in situ soil moisture and vegetation measurements at a U.S. Department of Agriculture (USDA) Natural Resources Conservation Service (NRCS) SCAN site in Lonoke, Arkansas (91.867°W and 34.833°N) (USDA, 2009a). The vegetation cover in the Lonoke area is primarily agricultural crops, including soybeans, rice, and wheat (Njoku et al., 2003). More than 1 year (1999–2000) of TMI passive microwave data at 10.7 and 19.3 GHz were analyzed, centered within 25 km of the Lonoke SCAN site. Results showed a wide range of sensitivity in the response of instantaneous PR (obtained at each local overpass time) and the transient SMC after rain events. The variance between measurements and linear fit values of daily PR (10.7 GHz) versus the contemporaneous daily m_v became so large at larger soil moisture values that PR varied by a factor of 3 at $m_v = 34\%$, while a transient soil moisture can change 6%–34% for the same PR value around 0.017. This is consistent with the findings by Njoku et al. (2003), which indicate that transient soil moisture events are not effectively captured by TMI data.

In contrast, seasonal trends in TMI PR (90 day running average) are well correlated with seasonal soil moisture (90 day running average) measured at a depth

TABLE 9.1
Correlation Results between Seasonal TMI PR and Seasonal SCAN Volumetric Soil Moisture m_v at 5 cm Depth from Linear Regression Analysis in the Form of $PR = \alpha \cdot m_v + \beta$ with a Correlation Coefficient ρ

	10.7 GHz			19.3 GHz		
	α	β	ρ	α	β	ρ
Fall–winter	0.00109	0.00766	0.977	0.000931	0.00587	0.953
Spring–summer	0.00131	-0.00108	0.988	0.000960	-0.000908	0.946
All year	0.00124	0.00235	0.936	0.000894	0.00320	0.792

of 5 cm at the Lonoke SCAN site (Table 9.1). Plots of seasonal data for contemporaneous SCAN m_v and TMI PR at both frequencies reveal a hysteresis behavior (Figure 9.1). Theoretically, Equation 9.1 suggests that the hysteresis is caused by attenuation effects on the passive microwave signatures under different vegetation conditions during different seasons. In Figure 9.1, the linear fit for all data in the entire year is used as a reference for each frequency. The PR generally lies above the annual linear fit during the fall and winter seasons of 1999 with vegetation cover decreasing in early fall, reaching a minimum in winter, and then increasing toward the spring equinox in 2000. In contrast, PR is mostly below the annual linear fit during spring and summer as the vegetation cover increases to a peak in summer and then slightly decreases toward the fall equinox. Vegetation attenuation effects cause the hysteresis in seasonal PR versus m_v observed at both frequencies with less severe impacts at the lower frequency evidenced by the smaller spread at 10.7 GHz around the best-fit line in Figure 9.1.

For the active microwave analysis, time-series QSCAT data were extracted within 25 km around the same SCAN site in the same manner as for the TMI data. In contrast to the passive microwave case, daily QSCAT backscatter change correlates well with contemporaneous SMC from rainwater. Daily QSCAT data capture 91% of the rain events recorded at the Lonoke SCAN site in 1999–2000. To illustrate the high correlation of QSCAT backscatter to transient soil moisture, a regression analysis using daily observations was performed for the period of October 4 to November 19, 1999, when two major rain events occurred over the SCAN site. With the linear formulation in the inverted form of Equation 9.5 such that $m_v = a' \cdot \sigma_0 + b'$ for backscatter σ_0 in dB, m_v in percent, and $a' = 8.9\%/dB$ and $b' = 111.1\%$, a high correlation coefficient of 0.91 and a small standard deviation of 3.7% were found for backscatter at the horizontal polarization (σ_{0HH}). This indicates that both the initial impulse of soil moisture increase from rain and the subsequent soil moisture decrease in the ensuing drying process were well represented. For backscatter at the vertical polarization (σ_{0VV}), the result is similar, with SMC of 8.4% for a dB change in σ_{0VV} , and thus the backscatter at the vertical polarization is slightly less sensitive than the horizontal polarization to transient soil moisture. This is consistent with Equation 9.4, where the dyadic Green’s function includes soil reflection, which is stronger at the horizontal polarization than

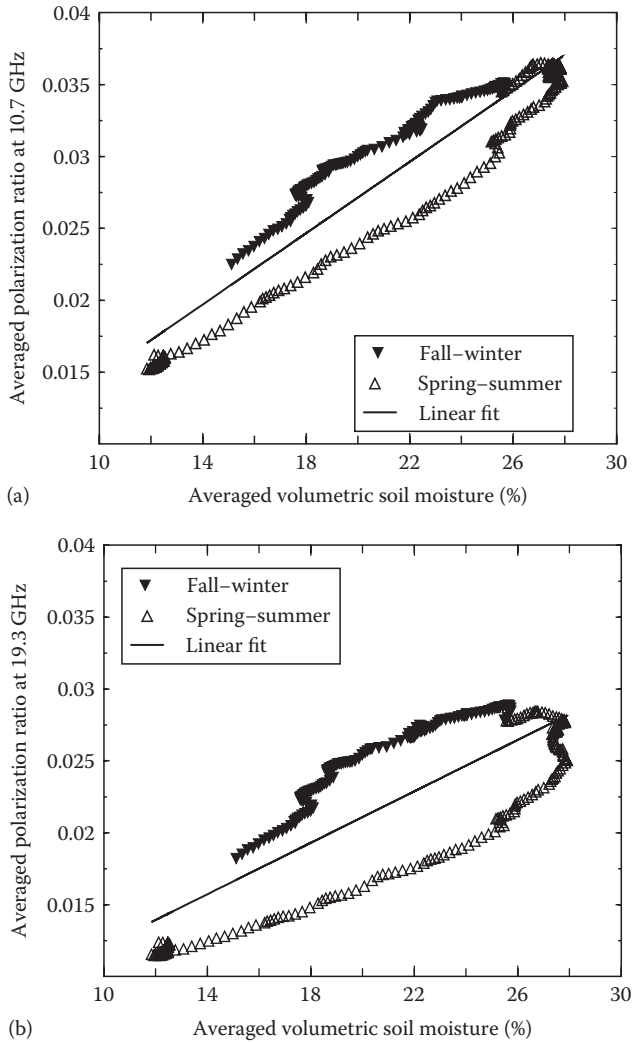


FIGURE 9.1 Seasonal TMI *PR* at (a) 10.7 GHz and (b) 19.3 GHz versus seasonal SCAN soil moisture at 5 cm depth in an agricultural area at Lonoke, Arkansas. All data are contemporaneous (collocated in time) and are 90 day running averages.

the vertical polarization. Also, the incidence angle at 54° for σ_{0VV} is larger than 46° for σ_{0HH} , which means that σ_{0VV} suffers from higher attenuation effects because of the longer path length in the vegetation cover. Nevertheless, QSCAT data can identify sufficiently heavy rainfall events even at peak vegetation conditions when the backscatter increases above the seasonal level of the background backscatter. As a result, QSCAT has the capability to identify transient SMC. This illustrates the complementary information that can be estimated from the combination of active and passive microwave data, together capturing both transient and seasonal trends in soil moisture content.

Seasonal trends in active backscatter data primarily convey information about vegetation. To demonstrate this, Normalized Difference Vegetation Index (NDVI) data representing seasonal vegetation change (Justice et al. 1985; Verdin et al., 1999; Zhang et al., 2010) were compared with seasonal QSCAT backscatter data (90 day running average). Advanced Very High Resolution Radiometer (AVHRR) NDVI data from the National Oceanic and Atmospheric Administration (NOAA) AVHRR were averaged within 25 km around the SCAN site so that the spatial scale of AVHRR NDVI data was compatible with the QSCAT data. A high correlation coefficient of 0.946 was found between the NDVI and linear σ_{0VV} and a slightly lower correlation coefficient of 0.864 between the NDVI and linear σ_{0HH} . Therefore, seasonal QSCAT backscatter can be used to characterize seasonal vegetation change regardless of cloud cover, which is transparent to QSCAT at the Ku-band frequency of 13.4 GHz. This is consistent with earlier results on the relation of Ku-band backscatter with NDVI (Moran et al., 1997), green leaf area index (Moran et al., 1998), and above-ground biomass (Nghiem, 2001).

Seasonal running averaged QSCAT σ_{0VV} (more sensitive to seasonal vegetation change compared to σ_{0HH}) and TMI PR at 10.7 GHz (more sensitive to seasonal SMC compared to 19.3 GHz data) were compared over the fall–winter season and spring–summer season. The hysteresis behavior is clearly observed in the curve of σ_{0VV} versus PR (Figure 9.2). In fall and winter, PR is below the annual linear fit, corresponding to less vegetation cover as compared to spring–summer PR above the linear fit with more vegetation cover. The lower vegetation cover indicated by lower backscatter in fall and winter supports the fact that PR is above the annual linear fit in the $PR-m$, hysteresis (Figure 9.1) for less vegetation attenuation effects on PR , and vice versa for spring and summer. We observe that the vegetation peak seen in σ_{0VV} occurs in summer after the seasonal soil moisture reaches the maximum seen in PR

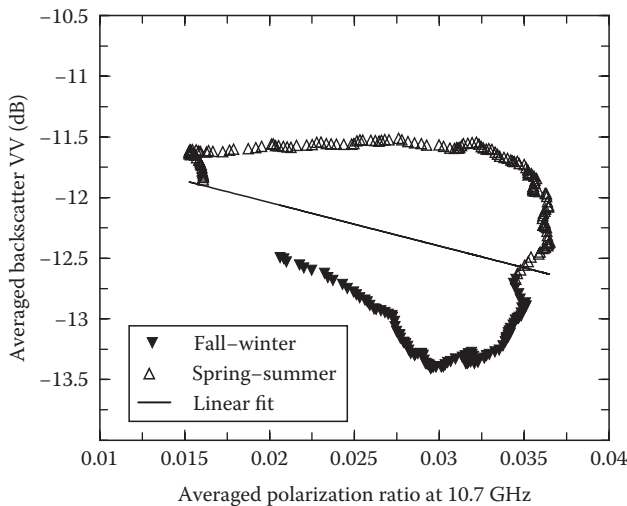


FIGURE 9.2 Seasonal QSCAT backscatter σ_{0VV} versus seasonal TMI PR at 10.7 GHz in an agricultural area within 25 km around Lonoke, Arkansas. All data are contemporaneous (collocated in time) and are 90 day running averages.

in spring. This analysis shows that independent information on seasonal vegetation change in active backscatter data can explain vegetation cover effects on passive microwave signatures.

9.3 DROUGHT APPLICATIONS

9.3.1 DROUGHT MONITORING ISSUES

For hydrological and agricultural drought assessment and monitoring, water on the land surface and in the soil are both relevant, and thus soil moisture data must play a key role. Nevertheless, the current in-situ station network is inadequate, and soil moisture measurements are too sparse for effective use or are nonexistent in many areas (NIDIS, 2007).

For county-level monitoring, which is an important goal of the National Integrated Drought Information System (NIDIS) (Western Governors' Association, 2004; NIDIS 2006, 2007), the National Weather Service (NWS) has determined that an effective Cooperative Observer Network would require a minimum spatial density of one observing site per 1000 km² across the country or a separation of about 24–32 km (NIDIS, 2007). The location of each in-situ sensor must be carefully selected such that the measured soil moisture is representative of the surrounding area. Furthermore, consistency and persistency in data collections are important in terms of data quality and data availability across different agencies and across different states.

9.3.2 USES OF SATELLITE DATA

In view of the aforementioned issues in drought monitoring, recent efforts have enabled certain uses of soil moisture measurements derived from satellite remote sensing data for enhancing drought monitoring systems (Nghiem et al., 2010). Several specific results are presented in this section to illustrate various uses of satellite data with different temporal and spatial scales.

9.3.2.1 Temporal Data at Local Scale

Temporal QSCAT observations combined with in-situ station measurements are used to illustrate how satellite data can help to enhance drought monitoring capabilities. [Figure 9.3](#) presents results at the NCDC Global Summary of the Day (GSOD) (NCDC, 2010a) Station 727760 in Great Falls, Montana (47.467°N, 111.383°W). Time series of QSCAT data together with in situ measurements around this station are constructed with the Special Satellite-Station Processor (SSSP) (Nghiem et al., 2003). Daily QSCAT data at horizontal polarization (more sensitive to soil moisture than vertical polarization) were selected with centroids located within 25 km around Station 727760 and from ascending orbits (~6 a.m. local overpass) that are better correlated with soil moisture than data from descending orbits.

QSCAT σ_{HH} data around Great Falls (top panel in [Figure 9.3](#)) clearly identify rain events before and after the dry period between July 9 and September 5, 2000, when very little rain fell. In August 2000, the long-term Palmer Drought Index for the

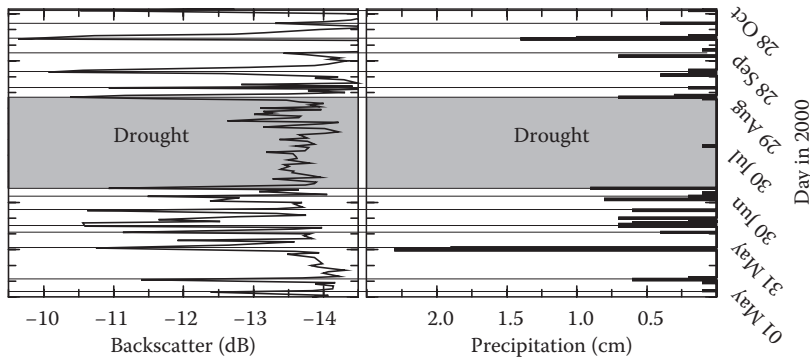


FIGURE 9.3 Measurements around the NCDC GSOD Station 727760 (47.467°N 111.383°W) at Great Falls in Montana. Left panel is QSCAT σ_{0HH} within 25 km around the station, and right panel is precipitation from station rain gauge. Thin horizontal lines align rain events to backscatter impulses. Gray shaded area defines the period between July 9 and September 5, 2000, when there was very little rainfall.

region around Great Falls was -4 or below, indicating long-term, extreme drought conditions. USDA issued Natural Disaster Determinations for drought for the entire state of Montana in 2000, when severe and persistent drought caused significant losses to agriculture and other sectors (Resource Management Services, 2004). The summer drought period observed by QSCAT is validated by the lack of rain in in situ precipitation data (right panel in Figure 9.3) for the same period, when several heat waves occurred. Both before and after this midsummer drought period, QSCAT detected a number of significant rain events that increased backscatter by about 3 dB, which is equivalent to a 26.8% increase in volumetric soil moisture (per the Lonoke rating value of $a' = 8.921\%/dB$). Thus, water from these rain events reached the land surface and significantly increased the moisture in soil. In contrast, rain gauge precipitation (RGP) data corresponding to these significant rain events inconsistently and disparately ranged across one order of magnitude from low values (<0.2 cm) to high values (>2.0 cm).

9.3.2.2 Spatial Data at Regional Scale

Satellite microwave remote sensing data, such as AMSR-E or QSCAT, can be used to monitor drought and water resources at regional to global scales. Both have swath widths of 1400 km or larger (Tsai et al., 2000; Njoku et al., 2003), which allow a near-daily global coverage and as many as two data acquisitions per day at high latitudes. Several attributes related to water can be obtained from microwave satellite data for drought monitoring. Examples of these information products derived from AMSR-E and QSCAT data are provided for 2009 over the state of Texas, when much of the state was afflicted by drought (Texas Water Development Board, 2007).

A relevant attribute for water resource and drought assessments is precipitation frequency, which quantifies the recurrence of rain events in a given period (González and Valdés, 2004). Instead of apparent precipitation frequency (APF), derived from in situ rain gauge data or surface rain radar data, a different measure of effective

precipitation frequency (EPF) can be derived from satellite scatterometer data. EPF accounts for rainwater that effectively reaches the land surface and increases soil moisture, as opposed to APF, which may have problems with apparent precipitation, virga, or inconsistency in gauge data collection. For applications to QSCAT data, $EPF = 100(N_w/N_c)$ is defined as the percentage of the number of wet days (N_w) when the soil moisture increase is $\geq 5\%$ in the topsoil layer (5 cm) such that the corresponding backscatter increase is ≥ 0.56 dB for σ_{0HH} or ≥ 0.60 dB for σ_{0VV} above the background level, over the total number of satellite coverage days (N_c) excluding days when satellite data were missing in a given period.

EPF was retrieved from QSCAT data across Texas from June 1 to August 31, 2009 (left panel in Figure 9.4). In summer 2009, exceptional drought occurred over much of south-central Texas, as shown in the U.S. Drought Monitor (USDM) maps from June to August 2009 (right panels in Figure 9.4). By August 2009, extreme and exceptional drought conditions (D3 and D4, respectively) remained persistent across south-central Texas, where the topsoil conditions were very dry and river levels were near historic lows (NCDC, 2009). Consistent with these drought conditions, QSCAT EPF showed few to no rain events across most of southern Texas (black to magenta areas, left panel of Figure 9.4). In contrast, soil in part of the Texas Panhandle was shown to be wetted by several rain events during this time period (light blue to green and yellow areas, left panel of Figure 9.4), which is reflected by the change of conditions in the USDM maps, which showed most of the area classified as abnormally dry (D0) in June had improved to no drought by late August 2009.

Although EPF carries information on wet precipitation frequency or how often the land surface becomes wet because of rainwater, daily SMC from QSCAT data

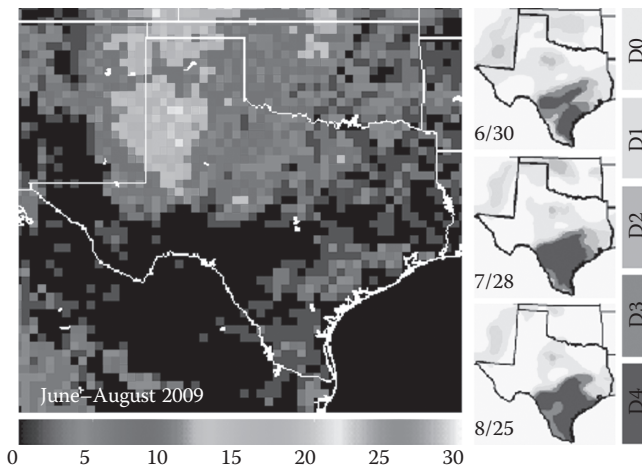


FIGURE 9.4 (See color insert.) Effective precipitation frequency (%) measured by QSCAT for the period June–August 2009 (left panel) and drought levels from D0–D4 from the USDM for weeks ending on the marked dates in 2009 (right panels). The USDM drought levels include D0 for abnormally dry, D1 for moderate drought, D2 for severe drought, D3 for extreme drought, and D4 for exceptional drought. (Ref. Svoboda et al. 2002.)

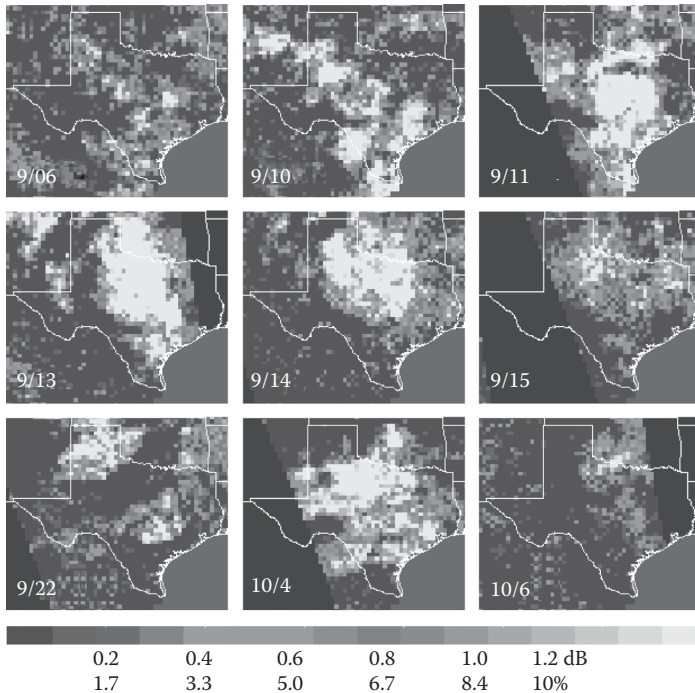


FIGURE 9.5 (See color insert.) SMC measured by QSCAT with the vertical polarization along ascending orbits in September to early October 2009. The color scale represents backscatter change in dB and volumetric SMC in % with the Lonoke rating.

represents the quantitative change in soil moisture or the amount (intensity) of rain-water that accumulates on land surface each day. Therefore, SMC is an attribute relevant to monitoring hydrological drought because it is related to water on land rather than raindrops in the atmosphere (a meteorological parameter). Hydrological drought is associated with shortfalls on surface or subsurface water supply whereas meteorological drought is related to deficiencies of precipitation (Wilhite and Glantz, 1985). SMC is also appropriate for early warning of agricultural drought (drought that has agricultural impacts) because SMC represents the source of rainwater that can infiltrate into the root zone after a rain event.

Figure 9.5 presents maps of selected daily SMC compared to the semimonthly average over Texas from early September to early October 2009. Intense SMC (in yellow), which reflects large increases in soil moisture, occurred across large areas of central Texas on September 10, 11, 13, and 14 and October 4. The SMC results on these days are consistent with torrential rainfall events reported across central and south Texas (up to 20 in. of total rainfall recorded in some locations) in September 2009, causing flash flooding (NWS, 2009). With this new water input, drought conditions in central and south Texas significantly improved by early October 2009 (as shown in the USDM map for October 6 in Figure 9.6).

Complementary to the transient change observed in the QSCAT daily SMC, AMSR-E passive microwave data provide good measurements of seasonal soil

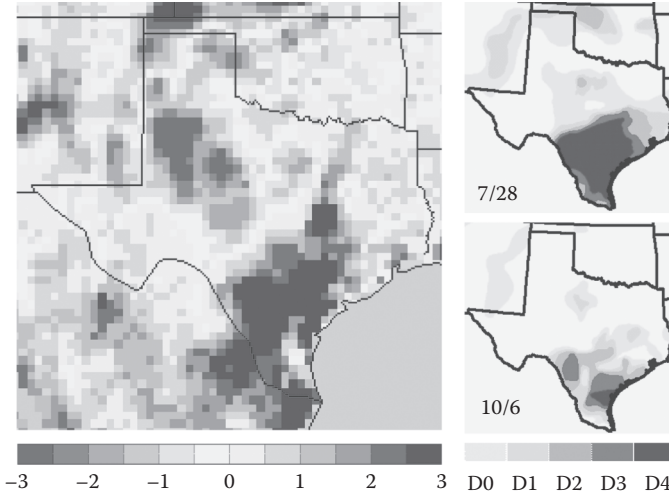


FIGURE 9.6 (See color insert.) Difference of AMSR-E monthly averaged soil moisture in % of m_v (September 7 to October 6, 2009) and m_v (June 29 to July 28, 2009) showing seasonal SMC (left panel), and drought condition change between USDM drought maps in July and in September 2009 (right panels).

moisture (as discussed in Section 9.2.3). Figure 9.6 (left panel) shows the difference in seasonal soil moisture between the June–July and September–October periods in 2009. AMSR-E seasonal soil moisture results reveal a large region of increased soil moisture in south-central Texas (blue areas). This corresponds to the marked improvement in drought conditions in September compared to those in July 2009 as depicted on the USDM drought maps (right panels in Figure 9.6). In contrast, an area in western Texas had a substantial reduction in soil moisture by the September–October period (red–brown areas in the left panel of Figure 9.6) compared to more moist conditions in the June–July period. This area had a larger EPF observed by QSCAT in the earlier months, as seen in the left panel of Figure 9.4 for June–August 2009.

The independent attributes derived from different remote sensing data sets (QSCAT and AMSR-E) are consistent with the changes in true drought conditions that occurred over Texas in 2009 and provide complementary perspectives for drought assessments. The improvement in drought conditions classified in the USDM map on October 6, 2009, (lower right panel in Figure 9.6) reflects the recent transient wetting events observed in daily SMC from QSCAT (e.g., SMC map for October 4, 2009, in Figure 9.5) and the seasonal SMC observed by AMSR-E (Figure 9.6). These results demonstrate the capability and consistency of different microwave-based parameters to depict the state of soil moisture, as well as its transient and seasonal changes from local to regional scales.

9.3.2.3 Spatial Data at Continental Scale

A major advantage of satellite data is its large spatial coverage at continental to global scales compared to local, surface in situ measurements from station networks.

Here, the pattern of SMC as observed by QSCAT and AMSR-E satellites is examined across the contiguous United States (CONUS) and compared to rainfall patterns from the regional multisensor precipitation analysis assembled into national maps of Stage-4 daily precipitation (SDP) available from the National Mosaic and Multi-Sensor Quantitative Precipitation Estimation algorithm (NMQ, 2009). This comparison is to identify the similarities as well as the differences between precipitation data and soil moisture data, which are relevant for monitoring different drought types (SDP for meteorological drought versus SMC for early warning of agricultural drought).

The large swaths of measurements by QSCAT and AMSR-E provide near-daily coverage over the CONUS. However, data gaps exist, and a full coverage of the entire CONUS is not possible every day, especially when ascending- and descending-orbit data are used separately. Figure 9.7 shows daily SMC maps in May 2009 from QSCAT ascending-orbit data (Figure 9.7a) at about 6 a.m. local overpass time and from AMSR-E descending-orbit data (Figure 9.7b) at about 1:30 a.m. local overpass time.

Overall, the patterns of daily SMC from QSCAT and AMSR-E are similar. Both reveal precipitation water on land surface in the Midwest and the Great Lakes states extending toward the northeastern United States, whereas most of the western United States was dry. An extensive wet region is observed across Kansas and Nebraska in both SMC maps (marked by the circles in Figure 9.7a and b). Interestingly, a well-defined dry area is detected by both QSCAT and AMSR-E just south of Lake Michigan along the Illinois–Indiana border. However, some discrepancies exist between the AMSR-E and QSCAT SMC results. First, the volumetric SMC observed by QSCAT can be more than 10% in various areas (yellow areas in Figure 9.7a), where AMSR-E SMC barely exceeds 5% (blue areas, Figure 9.7b). For example, the region east of Lake Ontario in New York had a large positive SMC (wet) in the QSCAT map while the AMSR-E SMC showed a slightly negative value (dry). These differences are not surprising given the better sensitivity of QSCAT data to transient SMC, as discussed earlier in Section 9.2.3.

In the case of the discrepancy between QSCAT and AMSR-E SMC in New York, it could be hypothesized that the difference was due to the different observation times of the two instruments (6 a.m. for QSCAT and 1:30 a.m. for AMSR-E). However, SDP maps indicate significant rainfall on May 27 continuing to May 28, 2009, in New York (Figure 9.7c and d). The lower sensitivity in AMSR-E data to transient SMC is likely the cause of the differences in the SMC results. The SDP map on May 28 (Figure 9.7c) also shows a large-scale overall pattern similar to the SMC observed by QSCAT and by AMSR-E (to a lesser degree) with band of heavier rainfall across the upper Midwest and Great Lakes region extending into the northeastern states. However, the SDP map on May 28 indicates no precipitation in Kansas and Nebraska where both QSCAT and AMSR-E detected rainwater on land surface resulting from the intense rainfall on the previous day (see the region marked by circles in Figure 9.7). This case illustrates that SMC can represent the rainwater accumulated from preceding strong precipitation events with the water still remaining in the top soil for some period of time after the rain events. As such, SMC is

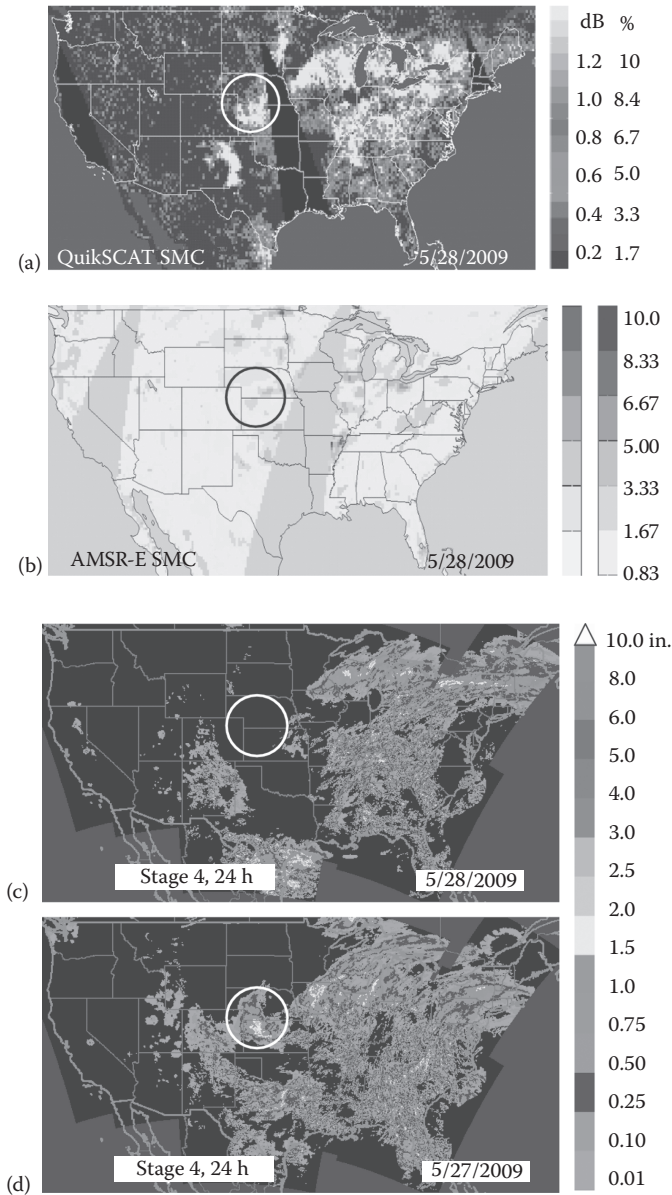


FIGURE 9.7 (See color insert.) SMC on May 28, 2009, compared to the 2-week average between May 14 and 28, 2009, observed by (a) QSCAT SMC represented by backscatter change in dB and by volumetric moisture change in % from the Lonoke rating, and (b) AMSR-E by volumetric moisture change in % with yellow brown for drier and cyan blue for wetter conditions. The SMC maps are compared with Stage-4 24h precipitation measurements (NMQ, 2009) at 12:00 UTC in inches for (c) May 28, 2009, and (d) and May 27, 2009.

also an indicator of the intensity or amount of rainwater on land surface (*vis-à-vis* rainwater as raindrops in the atmosphere) in terms of the SMC duration.

There are other discrepancies between SMC and SDP. For example, in New Mexico, SDP observed extensive precipitation across the state while SMC from both QSCAT and AMSR-E found wetness only in some areas of the state (such as in northeastern New Mexico). This difference suggests either the rainwater did not fully reach the land surface (*virga* problem) or SDP has uncertainties in surface radar data (AP problem). Similarly, the SDP pattern was much more widespread compared to the SMC pattern (Figure 9.7) in adjoining Texas, where AP problems can cause significant difficulties in precipitation mapping (Story, 2009). These observations suggest that SMC, pertaining to land surface conditions, is more relevant to hydrological and agricultural drought monitoring, while SDP as a parameter for precipitation rate is useful for meteorological drought monitoring. In the case of light rains, the small amount of rainwater that may reach the land surface can be evaporated before the next orbit pass, and thus SMC may not capture the wetness from light rains evaporated in a short time.

9.3.2.4 Soil Moisture Products for Drought Monitoring and Forecasting

In an operational environment, science results need to be transitioned into data and image products with appropriate formats and protocols that can be rapidly and easily used by drought experts, such as the USDM authors. Here, examples of various SMC products produced for the USDM are presented and compared with other traditional drought products to identify their advantages and limitations.

Three SMC attributes, including daily SMC, weekly maximum SMC, and weekly mean SMC, are produced and a USDM-defined color palette applied to classify the various levels of change. Because the USDM is an operational tool, the SMC data are updated weekly on Monday to be in sync with other updated products and analyses used to create the weekly USDM on Tuesday. The overall SMC processing system allows the flexibility in making SMC products with different time periods for various purposes, including the Monday-updated SMC for USDM operational assessment and 5–8 day SMC products for comparison and benchmarking with different NOAA precipitation maps.

Figure 9.8 presents an example of 8 day mean and 8 day maximum SMC maps, which are compared with the RGP product, representative of precipitation from October 14, 2008, and the ensuing 7 days. The RGP product is produced by NOAA's Climate Prediction Center (CPC) from several quality-controlled surface weather measurement data sources, including the Automated Surface Observing Systems (ASOS) and cooperative observers. Approximately 7000 daily in situ rain gauge observations are included in the making of the RGP product (Higgins et al., 2000). RGP maps are made with different time periods from 5 to 8 days for drought assessment. In this example, the full 8 day RGP product is compared with the corresponding 8 day SMC mean and maximum SMC maps (Figure 9.8a and b). In the maps, yellow to brown represent drier conditions and green to blue represent wetter conditions, which are shown with the corresponding USDM D-level contour lines for October 14, 2008.

The mean SMC map (Figure 9.8a) reveals a significant soil moisture increase (light blue area) extending in western Kansas, as well as a noticeable increase in soil moisture (green areas) in the Texas Panhandle, southeastern Texas, central Oklahoma, eastern New Mexico, and eastern Montana. Significant drying also appears across several states in the upper Midwest (Minnesota, Nebraska, and North and South Dakota). In comparison, the maximum SMC map (Figure 9.9b) indicates

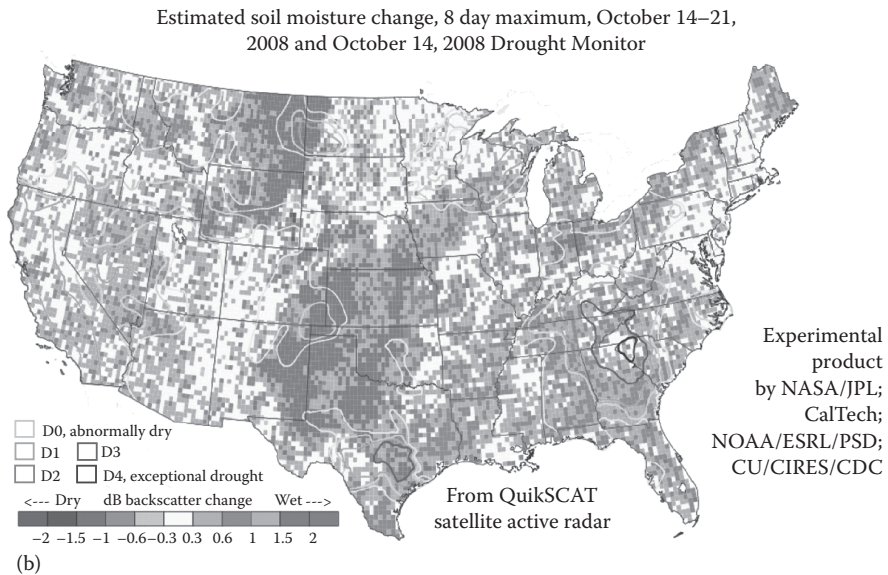
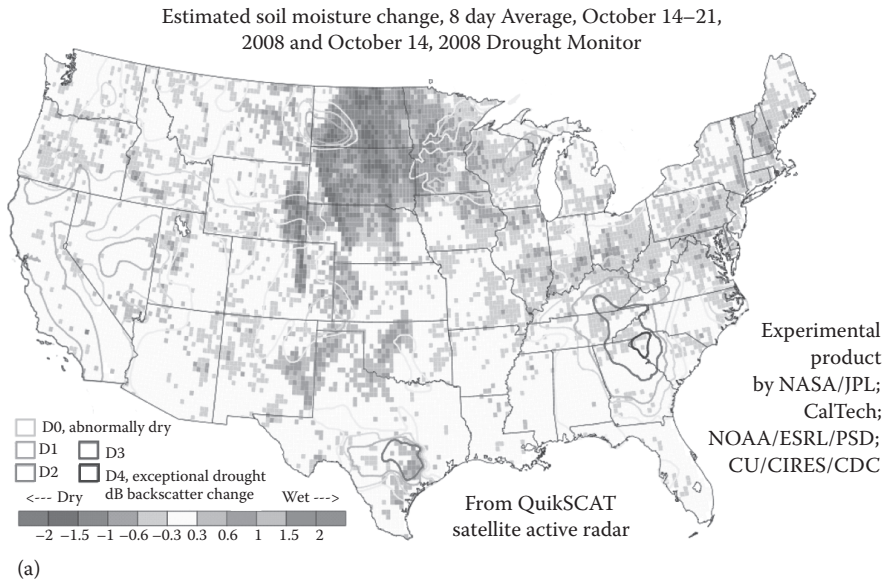


FIGURE 9.8 (See color insert.) Comparison of QSCAT SMC with RGP for the period of October 14, 2008, and the ensuing 7 days: (a) mean SMC, (b) max SMC, and

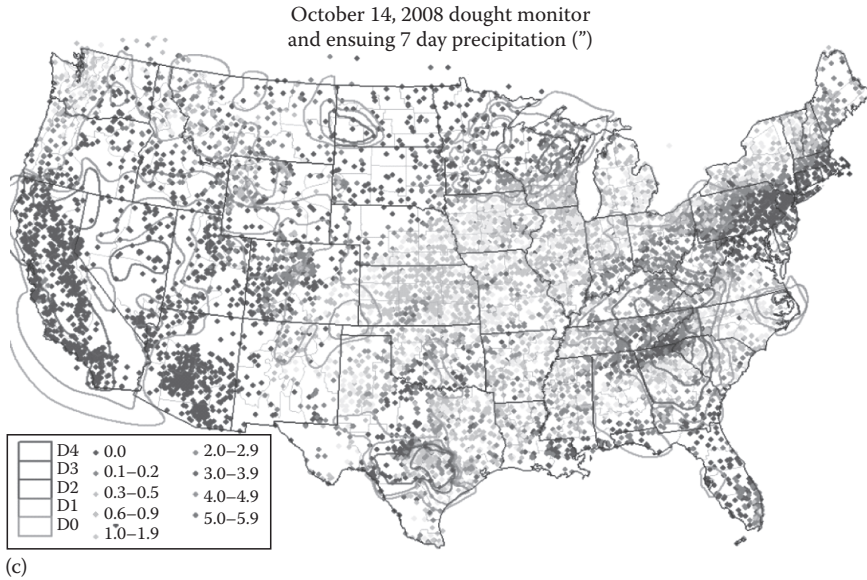


FIGURE 9.8 (continued) (See color insert.) (c) RGP used in making USDM maps.

a much more intensive soil moisture increase over extensive regions (blue to magenta areas) because it represents the peak soil moisture increase detected at any time in the 8 day period. The maximum SMC corresponds to the largest value of rainwater detectable on the land surface on any given day of the period including the remnant rainwater from previous days. In the maximum SMC map, a caveat is that low SMC values (gray and light green) are noisy because of spatial variability and limited accuracy in satellite data.

While the maximum SMC corresponds to the peak water accumulation on land surface, the mean SMC provides an assessment of the persistence of rainwater in soil, because the greater the number of days when a significant amount of soil moisture increase occurs, the larger the mean SMC value for that given time period. Therefore, it is possible to have a large peak SMC due to an intensive single-day rain event over an area (e.g., blue area between Indiana and Ohio in Figure 9.8b) where the maximum SMC value is high but the mean SMC is low because no rainwater accumulated on the other days during the 8 day period. Since the persistence of SMC (i.e., how long rainwater accumulates and remains in soil) depends on factors such as soil type, infiltration rate, and runoff processes, the mean SMC carries information that is relevant for hydrological and agricultural drought monitoring. The mean and the maximum SMC carry different information, and both can contribute to drought assessments.

For benchmarking, the traditional RGP product used in USDM is included in Figure 9.8c to compare with the mean and maximum SMC products. A comparison of the RGP and SMC maps clearly points to the different characteristics of these measurements: RGP consists of point data at separate rain gauge station locations, while the SMC maps are composed of 25 km pixels that provide continuous

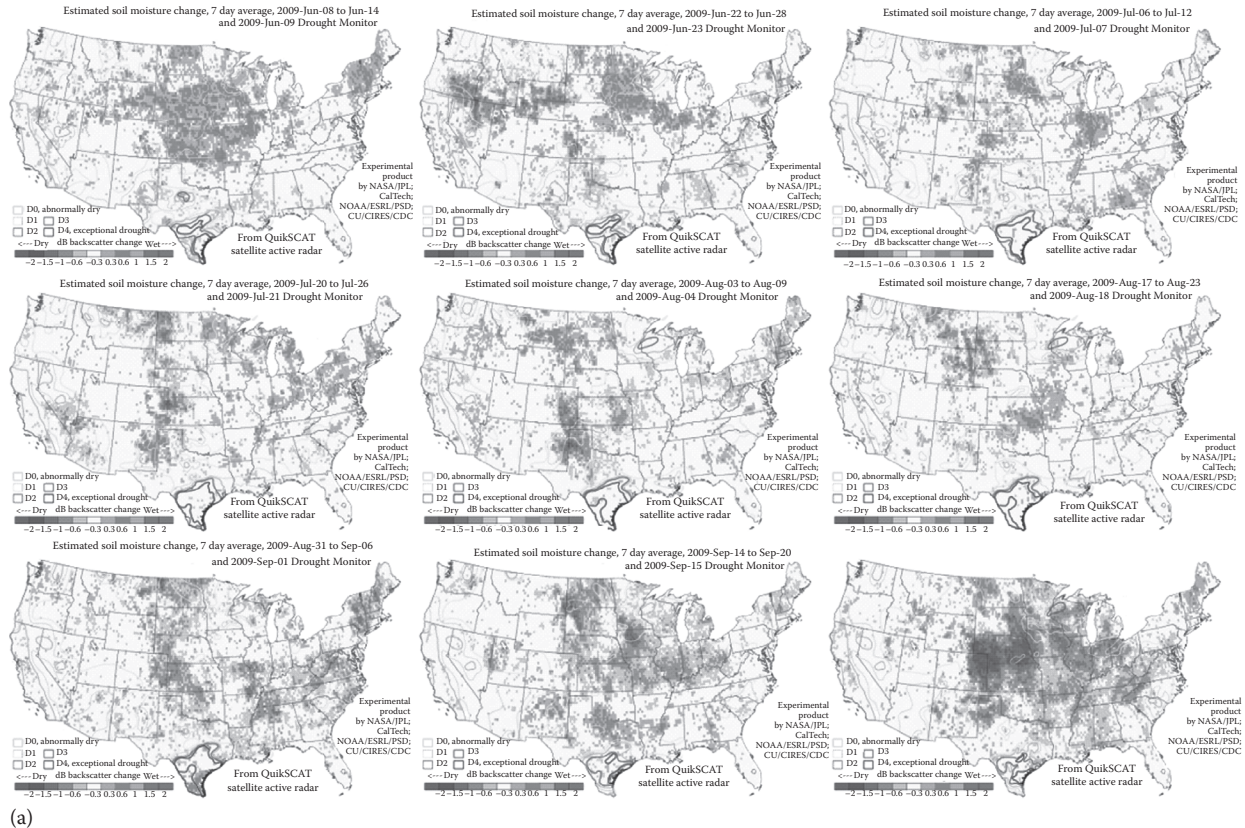


FIGURE 9.9 (See color insert.) Weekly QSCAT mean SMC maps (a) and USDM maps (b) for the growing season in June–October 2009 (skipping a map once every other week).

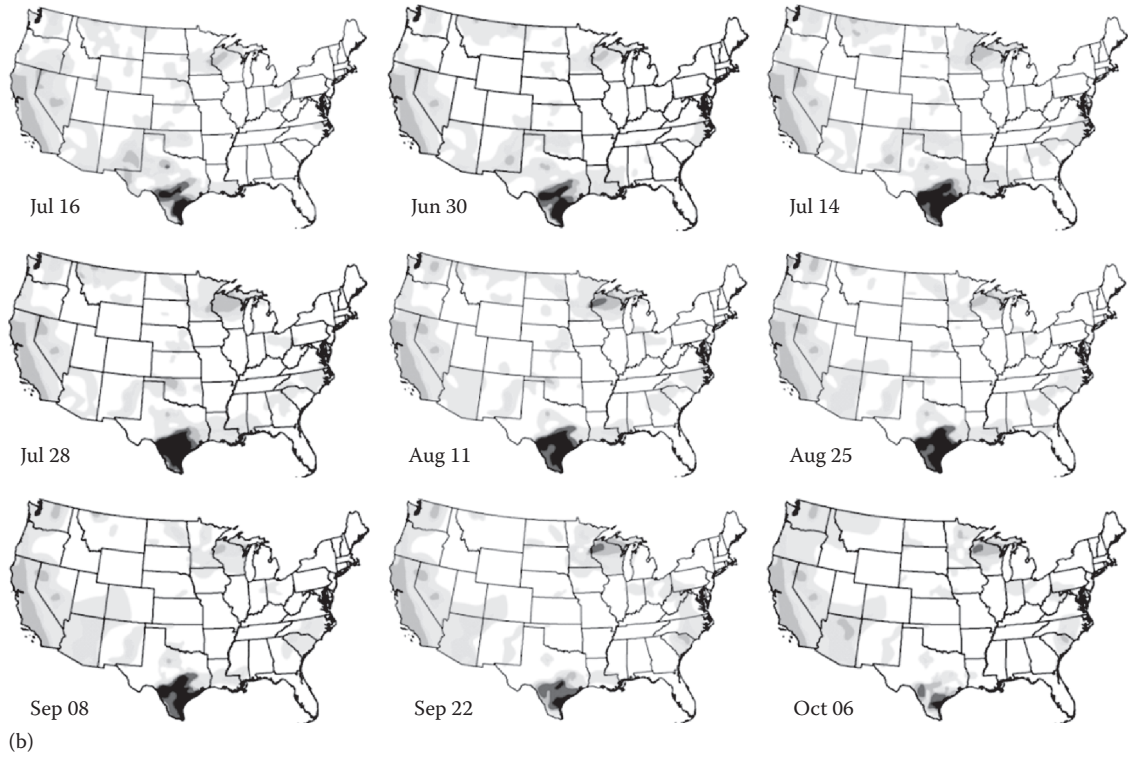


FIGURE 9.9 (continued)

spatial coverage of measurements across the CONUS. The vastly improved spatial coverage at an appropriate resolution of the satellite observations is important for resolving the county-level drought condition, which is currently lacking for most inputs into the USDM and is a goal of NIDIS. The average county size for the CONUS is approximately 50 km in linear scale ($\sim 2500 \text{ km}^2$ in area) as estimated from census data (U.S. Census Bureau, 2005). Thus, to resolve information at the 50 km county scale, a spatial scale of 25 km is required according to the Nyquist sampling theorem, which is satisfied by the SMC data. However, RGP can provide more frequent hourly data, whereas the SMC is only available two times per day at most. Although the SMC temporal scale is suitable for the weekly USDM, better temporal coverage can improve the overall result, especially in the tropics, where current satellite data gaps are the largest because of the divergence of satellite swaths at lower latitudes.

Although the spatial patterns in both RGP and maximum SMC maps (Figure 9.8b and c) agree in general over the areas of extensive precipitation discussed earlier, a large area of discrepancy exists over Montana, Wyoming, and part of North Dakota. This discrepancy is primarily due to the SMC having a memory of any precipitation water as long as it remains on land surface at the time of the satellite measurement (as in the cases presented in Figure 9.7 with a comparison of SMC to precipitation data) as opposed to the instantaneous and temporally discrete rain gauge measurements at specific station location. These results point out a key advantage of SMC in “memorizing” the rainwater staying on land surface integrated up to the time of measurement, allowing less frequent SMC measurements to capture the state of soil moisture. In contrast, satellite precipitation measurements need to be very frequent to capture the amount of rainwater falling through the atmosphere at the exact discrete time of each precipitation event.

Regarding the mean SMC (Figure 9.8a), a high value requires sufficient rainwater to accumulate on land surface over a significant duration during the period under consideration. The mean SMC represents both the quantity and persistence of new precipitation water in soil, which is more relevant to drought monitoring than both maximum SMC and RGP. For example, maximum SMC and RGP identify a precipitation pattern in eastern Nebraska and Iowa; however, the same region appears dry in the mean SMC. This indicates that the transient rainwater may not have been sufficient to sustain the presence of soil moisture over a significant fraction of the 8 day period to have an overall impact on soil moisture condition over the given period.

For the 2009 growing season (i.e., June to early October), Figure 9.9 presents a comparison of QSCAT SMC and USDM results across the CONUS. There is an overall consistency between the two sets of results on a regional scale. This is observed as a monitoring process in detecting the frequency, intensity, and extent of SMC rather than an isolated examination of the spatial pattern in each map at a given time. For example, throughout the 2009 growing season, not much water from precipitation was detected on land surface, as seen in the SMC maps in the West and the Southwest, where USDM maps consistently show either no improvement (e.g., California) or worsening drought conditions (e.g., Arizona). For south Texas, no significant wet events occurred in the first part of the growing season,

which is reflected by the severe to extreme drought conditions in the USDM, while the rainfall events in August and September that improved the drought conditions (as shown in the USDM maps in September and early October) are represented by the positive SMC in September.

In the Midwest, [Figure 9.9](#) reveals extensive SMC in South Dakota, southern Minnesota, eastern Nebraska, and western Iowa in June and July 2009. During this same time period, USDM results consistently indicate some improvement in South Dakota, Nebraska, and Iowa (primarily change from D0 to no drought classification), and USDM maps suggest drought levels in Minnesota remained the same or became slightly worse. In early June 2009, SDP results showed an extensive rain pattern over the Midwest, including Minnesota, which suggests that rainwater was still present on the land surface as detected in the SMC (top left panel in [Figure 9.9](#)). Since the mean SMC represents a persistent amount of rainwater on land, SMC inherently reflects information about temperature, wind, insolation, and other parameters that affect soil wetness. Therefore, SMC may supplement information in synergy with other parameters currently used in the USDM to enhance the results.

SMC as measured by satellite can benefit not only drought monitoring but also drought forecasting. Skillful forecasts of drought or soil moisture would have significant uses for agriculture and hydrology (water planning). Recognizing the importance of seasonal forecasts of drought, NOAA CPC has been issuing such forecasts since March 2000. These forecasts are designed to indicate whether existing droughts will persist or improve and whether a new drought will form. An important first step in creating an improved forecast would be better knowledge of existing conditions. The SMC, as shown in [Figures 9.8](#) and [9.9](#), is an appropriate parameter to contribute to a more accurate depiction of near-surface moisture supplies.

9.4 SUMMARY AND CONCLUDING REMARKS

Soil moisture derived from active and passive microwave remote sensing data can be used to enhance drought monitoring capabilities as summarized in the following:

1. SMC from active scatterometer data can characterize transient changes including the intensity, frequency, and extent of rainwater that actually reaches and accumulates on land surface, whereas passive radiometer data are for seasonal soil moisture. Together, soil moisture measurements from active and passive satellite data represent the state of dryness or wetness pertaining to land surface and are thus relevant to both hydrological and agricultural drought, as opposed to precipitation data (such as the specific precipitation index), which is more relevant to meteorological drought (WMO, 2009).
2. Satellite soil moisture measurements from scatterometer and radiometer data have continuous coverage across large geographic areas, whereas in situ RGP data or soil moisture networks such as SCAN consist of a relatively sparse spatial distribution of point data from networks with varying station densities and different data quality standards. Also, in the weekly

time scale for drought monitoring by the USDM and NIDIS, both QSCAT and AMSR-E data have a full coverage of the CONUS.

3. Satellite areal data represent the condition over the whole pixel size as opposed to a single local site at each in situ station. Moreover, QSCAT data with a 25 km resolution satisfy the Nyquist requirement to resolve the county-level drought condition, which is currently lacking for most inputs into the USDM and is an important goal of NIDIS.

Nevertheless, satellite measurements also have limitations, which necessitate using them in combination with in situ observations to more fully characterize soil moisture conditions. For example, in situ measurements can be obtained many times in a day (e.g., hourly measurements), whereas a satellite sensor typically collects data one or two times per day depending on the latitude. In addition, many in situ stations have a longer observational time series compared to satellite data. In particular, AMSR-E data have been collected since 2002 (starting in October 2011, the AMSR-E instrument was no longer operational), and QSCAT data were obtained over a decade (1999–2009), while many rain gauge stations were established several decades ago. Furthermore, there are differences in the characteristics of attributes measured by in situ gauges and by satellite sensors as presented in the benchmark study in the previous section, which should be combined to better represent various drought conditions.

For in situ data to be more useful, in situ measurements should characterize the conditions as far as possible beyond the local site. Here, satellite data can assist in the assessment of the extent beyond which local measurements are valid. For example, soil moisture data from SCAN can be compared or correlated in time (across months, seasons, or years) to satellite soil moisture signatures collected over areas with different radii away from the in situ station, to determine whether and how far the different measurements are correlated. The larger the radius at which satellite data and in situ measurements are well correlated, the larger the extent to which in situ data are representative. This is valuable in the selection of station locations for long-term maintenance so that the surface data are valid over the largest area as possible (not just in a close proximity of each station), thereby minimizing the number of stations required to monitor a certain region such as a county (in view of the county-scale goal of NIDIS).

Assimilation systems (Mitchell et al., 2004; Kumar et al., 2008) can be used to integrate various ground measurements and satellite observations within an ensemble framework of community land-surface models. This modeling approach allows data with various time scales and spatial coverage to be incorporated in a systematic manner. Because in situ networks are changing and improving and new satellite data and products are being developed, land data assimilation systems need to continuously evolve to provide enhanced products for drought monitoring. Furthermore, new measurements can allow better cross-verifications and validations among different models used in the land data assimilation systems in an effort to produce accurate, high-quality products.

Drought is a common climatic phenomenon throughout the world and a global problem requiring international efforts for drought assessment, forecasting, and mitigation. In this regard, satellite data from different nations can contribute to this overall goal. The QSCAT antenna ceased to spin in November 2009 after its continuous operation

since July 1999. Meanwhile, the Indian Space Agency successfully launched another scatterometer similar to QSCAT aboard the Oceansat-2 Satellite (OSCAT) (Jayaraman et al., 1999) in September 2009. These satellite events, together with a scatterometer data agreement signed among the different nations, highlight the importance of international collaborations in improving global satellite coverage for drought monitoring.

As of December 2011, QSCAT is still measuring valid backscatter data along narrow tracks at a fixed azimuth, which are valuable for validating OSCAT measurements. Once verified with QSCAT, OSCAT can continue the QSCAT time series of SMC. A long-term SMC record is important for assessing drought conditions within the climatic historical perspective. In August 2011, China launched the Haiyan-2 (HY-2) satellite carrying another scatterometer (Dong et al., 2004). In addition, the development of another advanced satellite scatterometer is being studied in the United States, stemming from the recommendation of the NRC Decadal Survey (National Research Council, 2007). The current European SMOS mission (Kerr et al., 2010) and the proposed NASA Soil Moisture Active and Passive (SMAP) mission (Entekhabi et al., 2010) could potentially provide global soil moisture measurements critical for drought monitoring. Collectively, these successive satellite missions would provide multidecadal data important for addressing the nonstationarity issue in climate change. Moreover, long-term data are necessary for developing a probabilistic standardized index approach with multiple time scales of soil moisture variability that could be used for drought monitoring.

Experiences in using microwave satellite data to enhance the USDM will be valuable in improving international drought monitoring systems, such as the North American Drought Monitor (NADM) covering Canada, Mexico, and the United States (NCDC, 2010b). In developing countries that lack in situ or surface measurement networks, the role of satellite data for drought monitoring becomes increasingly important because products such as AMSR-E soil moisture and QSCAT SMC can be retrieved globally and fill informational gaps that are currently pervasive. Such products can enhance global drought monitoring, for which the Global Earth Observation System of Systems (GEOSS) (Lautenbacher, 2006) will be crucial as an overall integrator.

Long-term satellite-based moisture records are also important for developing climatologies used in forecasting drought conditions. Given the limited skill of seasonal forecasts of temperature and precipitation, drought forecasters place considerable weight on projecting current conditions forward based on what has happened in the past. In this regard, careful attention should be paid to the issue of nonstationarity due to significant changes in regional climatic trends in recent years. Improved knowledge of short-term moisture trends can contribute positively to drought forecasts. Although there is no guarantee that short-term trends will persist, forecasters need to know whether and how fast moisture conditions are deteriorating. Such trends serve to flag situations that require additional analysis. Once the SMC products are obtained for a suitable number of years to capture contemporary changes, forecasters may gain new knowledge of the probabilities that soil moisture conditions will likely improve or deteriorate during the following season. One of the goals of drought forecasting is to formulate the forecasts in terms of probabilities to provide a more accurate portrayal of confidence levels, and the statistics of historical soil moisture conditions can contribute to this effort. In short, improved knowledge of initial moisture conditions,

short-term trends, and climatology have the potential to enhance the skill of current and future drought forecasts globally as well as in the United States.

ACKNOWLEDGMENTS

The research carried out at the Jet Propulsion Laboratory, California Institute of Technology, was supported by the National Aeronautics and Space Administration (NASA) Water Resources Area of the NASA Applied Sciences Program. Thanks to Robert Rabin from the NOAA National Severe Storms Laboratory for his direction in acquiring Stage-4 daily precipitation products for comparison with SMC patterns.

REFERENCES

- Blanchard, B.J. and A.T.C. Chang. 1983. Estimation of soil-moisture from SEASAT-SAR data. *Water Resources Bulletin* 19(5):803–810.
- Cognard, A.L., C. Loumagne, M. Normand, P. Olivier, C. Ottele, D. Vidalmadjar, S. Louhala, and A. Vidal. 1995. Evaluation of the ERS-1 synthetic aperture radar capacity to estimate surface soil-moisture—2-Year results over the Naizin watershed. *Water Resources Research* 31(4):975–982.
- Dobson, M.C., F.T. Ulaby, M.T. Hallikainen, and M.A. Elrayes. 1985. Microwave dielectric behavior of wet soil, Part II: Dielectric mixing models. *IEEE Transactions on Geoscience and Remote Sensing* GE-23(1):35–46.
- Dong, X., K. Xu, H. Liu, and J. Jiang. 2004. The radar altimeter and scatterometer of China's HY-2 satellite. *Proceedings of IEEE International Geoscience and Remote Sensing Symposium* 3:1703–1706.
- Dubois, P., J.J. van Zyl, and T. Engman. 1995. Measuring soil moisture with imaging radars. *IEEE Transactions on Geoscience and Remote Sensing* 33(4):916–926.
- Engman, E.T. 1995. Recent advances in remote-sensing in hydrology. *Reviews of Geophysics* 33(Part 2, Supplement S):967–975.
- Entekhabi, D., E.G. Njoku, P.E. O'Neill, K.H. Kellogg, W.T. Crow, W.N. Edelstein, J.K. Entin, S.D. Goodman, T.J. Jackson, J. Johnson, J. Kimball, J.R. Piepmeier, R.D. Koster, N. Martin, K.C. McDonald, M. Moghaddam, S. Moran, R. Reichle, J.C. Shi, M.W. Spencer, S.W. Thurman, L. Tsang, Leung, and J.J. Van Zyl. 2010. The soil moisture active passive (SMAP) mission. *Proceedings of the IEEE* 98(5):704–716.
- González, J. and J.B. Valdés. 2004. The mean frequency of recurrence of in-time-multidimensional events for drought analyses. *Natural Hazards and Earth System Science* 4(1):17–28.
- van de Griend, A.A. and M. Owe. 1994. Microwave vegetation optical depth and inverse modelling of soil emissivity using Nimbus/SMMR satellite observations. *Meteorology and Atmospheric Physics* 54:225–239.
- Hallikainen, M.T., F.T. Ulaby, M.C. Dobson, M.A. El-Rayes, and L.-K. Wu. 1985. Microwave dielectric behavior of wet soil, Part I: Empirical models and experimental observations. *IEEE Transactions on Geoscience and Remote Sensing* GE-23(1):25–34.
- Higgins, R.W., W. Shi, E. Yarosh, and R. Joyce. 2000. Improved United States precipitation quality control system and analysis. *NCEP/Climate Prediction Center ATLAS No. 7*, U.S. Department of Commerce, National Weather Service, NOAA. http://www.cpc.noaa.gov/products/outreach/research_papers/ncep_cpc_atlas/7/ (last accessed on December 15, 2011).
- Hutchinson, J.M.S. 2003. Estimating near-surface soil moisture using active microwave satellite imagery and optical sensor inputs. *Transactions of the American Society of Agricultural and Biological Engineers (ASABE)* 46(2):225–236.

- Illston, B.G., J.B. Basara, and K.C. Crawford. 2004. Seasonal to interannual variations of soil moisture measured in Oklahoma. *International Journal of Climatology* 24:1883–1896.
- Jackson, T.J. 1990. Laboratory evaluation of a field-portable dielectric soil-moisture probe. *IEEE Transactions on Geoscience and Remote Sensing* 28(2):241–245.
- Jackson, T.J. 1997. Soil moisture estimation using SSM/I satellite data over a grassland region. *Water Resources Research* 33:1475–1484.
- Jayaraman, V., V.S. Hedge, M. Rao, and H.H. Gowda. 1999. Future earth observation missions for oceanographic applications: Indian perspectives. *Acta Astronautica* 44(7–12):667–674.
- Justice, C.O., J.R.G. Townshend, B.N. Holben, and C.J. Tucker. 1985. Analysis of the phenology of global vegetation using meteorological satellite data. *International Journal of Remote Sensing* 6(8):1271–1318.
- Kerr, Y.H. and E.G. Njoku. 1990. A semiempirical model for interpreting microwave emission from semiarid land surfaces as seen from space. *IEEE Transactions on Geoscience and Remote Sensing* 28:384–393.
- Kerr, Y.H., P. Waldteufel, J.P. Wigneron, S. Delwart, F. Cabot, J. Boutin, M.J. Escorihuela, J. Font, N. Reul, C. Gruhier, S.E. Juglea, M.R. Drinkwater, A. Hahne, M. Martin-Neira, and S. Mecklenburg. 2010. The SMOS mission: New tool for monitoring key elements of the global water cycle. *Proceedings of the IEEE* 98(5):666–687.
- Kerr, Y.H., P. Waldteufel, J.-P. Wigneron, J.-M. Martinuzzi, J. Font, and M. Berger. 2001. Soil moisture retrieval from space: The soil moisture and ocean salinity (SMOS) mission. *IEEE Transactions on Geoscience and Remote Sensing* 39(8):1729–1735.
- Kumar, S.V., R.H. Reichle, C.D. Peters-Lidard, R.D. Koster, X.W. Zhan, W.T. Crow, J.B. Eylander, and P.R. Houser. 2008. A land surface data assimilation framework using the land information system: Description and applications. *Advances in Water Resources* 31(11):1419–1432.
- Lautenbacher, C.C. 2006. The Global Earth Observation System of Systems: Science serving society. *Space Policy* 22(1):8–11.
- Li, Q., L. Tsang, J. Shi, and C.H. Chan. 2000. Application of physics-based two-grid method and sparse matrix canonical grid method for numerical simulations of emissivities of soils with rough surfaces at microwave frequencies. *IEEE Transactions on Geoscience and Remote Sensing* 38:1635–1643.
- Loew, A., R. Ludwig, and W. Mauser. 2006. Derivation of surface soil moisture from ENVISAT ASAR wide swath and image mode data in agricultural areas. *IEEE Transactions on Geoscience and Remote Sensing* 44(4):889–899.
- Maddox, R.A., J. Zhang, J.J. Gourley, and K.W. Howard. 2002. Weather radar coverage over the contiguous United States. *Weather and Forecasting* 17:927–934.
- Mitchell, K.E., D. Lohmann, P.R. Houser, E.F. Wood, J.C. Schaake, A. Robock, B.A. Cosgrove, J. Sheffield, Q.Y. Duan, L.F. Luo, R.W. Higgins, R.T. Pinker, J.D. Tarpley, D.P. Lettenmaier, C.H. Marshall, J.K. Entin, M. Pan, W. Shi, V. Koren, J. Meng, B.H. Ramsay, and A.A. Bailey. 2004. The multi-institution North American Land Data Assimilation System (NLDAS): Utilizing multiple GCIP products and partners in a continental distributed hydrological modeling system. *Journal of Geophysical Research* 109(D7):D07S90, doi:10.1029/2003JD003823.
- Mo, T., T.J. Schmugge, and T.J. Jackson. 1984. Calculations of radar backscattering coefficient of vegetation covered soils. *Remote Sensing of Environment* 15:119–133.
- Moran, M.S., A. Vidal, D. Troufleau, Y. Inoue, and T.A. Mitchell. 1998. Ku- and C-band SAR for discriminating agricultural crop and soil conditions. *IEEE Transactions of Geoscience and Remote Sensing* 36:265–272.
- Moran, M.S., V. Vidal, D. Troufleau, J. Qi, T.R. Clarke, P.J. Pinter, Jr., T.A. Mitchell, Y. Inoue, and C.M.U. Neale. 1997. Combining multifrequency microwave and optical data for crop management. *Remote Sensing of Environment* 61:96–109.

- National Research Council. 2007. *Earth Science and Applications from Space: National Imperatives for the Next Decade and Beyond*. Washington, DC: The National Academies Press.
- NCDC. 2009. *State of the Climate—Drought, August 2009*. National Climatic Data Center, NESDIS, NOAA, U.S. Department of Commerce. <http://www.ncdc.noaa.gov/sotc/?report=drought&year=2009&month=8> (last accessed on December 15, 2011).
- NCDC. 2010a. Global surface summary of the day—GSOD. National Climatic Data Center, NESDIS, NOAA, U.S. Department of Commerce. <http://www.data.gov/geodata/g600037/> (last accessed on December 15, 2011).
- NCDC. 2010b. North American drought monitor. National Climatic Data Center, NESDIS, NOAA, U.S. Department of Commerce. <http://www.ncdc.noaa.gov/temp-and-precip/drought/nadm/index.html> (last accessed on December 15, 2011).
- Nghiem, S.V. 2001. Advanced scatterometry for geophysical remote sensing. In *Jet Propulsion Laboratory (JPL) Document D-23048*. Pasadena, CA: Jet Propulsion Laboratory, California Institute of Technology.
- Nghiem, S.V., M. Borgeaud, J.A. Kong, and R.T. Shin. 1990. Polarimetric remote sensing of geophysical media with layer random medium model. In *Progress in Electromagnetics Research—Polarimetric Remote Sensing*. Vol. 3, ed. J.A. Kong, pp. 1–73. New York: Elsevier.
- Nghiem, S.V., R. Kwok, S.H. Yueh, and M.R. Drinkwater. 1995. Polarimetric signatures of sea ice, 1, Theoretical model. *Journal of Geophysical Research* 100(C7):13665–13679.
- Nghiem, S.V., T. Le Toan, J.A. Kong, H.C. Han, and M. Borgeaud. 1993a. Layer model with random spheroidal scatterers for remote sensing of vegetation canopy. *Journal of Electromagnetic Waves and Applications* 7(1):49–76.
- Nghiem, S.V., E.G. Njoku, G.R. Brakenridge, and Y. Kim. 2005. Land surface water cycles observed with satellite sensors. *Proceedings of the 19th Conference on Hydrology and 16th Conference on Climate Variability and Change, 85th American Meteorological Society Meeting*. San Diego, CA, January 9–13.
- Nghiem, S.V., E.G. Njoku, J.J. Van Zyl, and Y. Kim. 2003. Global energy and water cycle—Soil moisture variability pattern over continental extent observed with active and passive satellite data. In *Jet Propulsion Laboratory (JPL) Document D-26225*. Pasadena, CA: Jet Propulsion Laboratory, California Institute of Technology.
- Nghiem, S.V., J.J. Van Zyl, W.-Y. Tsai, and G. Neumann. 2000. Potential application of scatterometry to large-scale soil moisture monitoring. In *Jet Propulsion Laboratory (JPL) Document D-19523*. Pasadena, CA: Jet Propulsion Laboratory, California Institute of Technology.
- Nghiem, S.V., J. Verdin, M. Svoboda, D. Allured, J. Brown, B. Liebmann, G. Neumann, E. Engman, and D. Toll. 2010. Improved drought monitoring with NASA satellite data. *Environmental and Water Resources Institute (EWRI) Currents* 12(3):7.
- Nghiem, S.V., S.H. Yueh, R. Kwok, and D.T. Nguyen. 1993b. Polarimetric remote sensing of geophysical medium structures. *Radio Science* 28(6):1111–1130.
- NIDIS. 2006. National integrated drought information system act of 2006. Public Law 109–430. *U.S. Statutes at Large* 120(2006):2918. <http://www.gpo.gov/fdsys/pkg/PLAW-109publ430/pdf/PLAW-109publ430.pdf> (last accessed on December 15, 2011).
- NIDIS. 2007. The national integrated drought information system implementation plan—A pathway for national resilience. <http://www.drought.gov/pdf/NIDIS-IPFinal-June07.pdf> (last accessed on December 15, 2011).

- Njoku, E. 2004. *AMSR-E/Aqua L2B Surface Soil Moisture, Ancillary Params, & QC EASE-Grids V002*. Boulder, Co: National Snow and Ice Data Center. http://nsidc.org/data/docs/daac/ae_land_l2b_soil_moisture.gd.html (last accessed on December 15, 2011).
- Njoku, E.G., T.J. Jackson, V. Lakshmi, T.K. Chan, and S.V. Nghiem. 2003. Soil moisture retrieval from AMSR-E. *IEEE Transactions on Geoscience and Remote Sensing* 41(2):215–229.
- Njoku, E.G. and L. Li. 1999. Retrieval of land surface parameters using passive microwave measurements at 6–18 GHz. *IEEE Transactions on Geoscience and Remote Sensing* 37:79–93.
- NMQ. 2009. Stage-4 24hr QPE accumulation. National Mosaic & Multi-Sensor QPE (NMQ). OK: NOAA National Severe Storms Laboratory, Norman. <http://nmq.ou.edu/> (last accessed on December 15, 2011).
- NWS. 2009. September 2009 weather in review. NOAA National Weather Service (NWS), Southern Region Headquarters. <http://www.srh.noaa.gov/images/ewx/wxevent/sep2009.pdf> (last accessed on December 15, 2011).
- Owe, M., A. Chang, and R.E. Golus. 1988. Estimating surface soil moisture from satellite microwave measurements and a satellite-derived vegetation index. *Remote Sensing of Environment* 24:131–345.
- Prevot, M., M. Dechambre, O. Taconet, D. Vidal-Madjar, M. Normand, and S. Galle. 1993. Estimating the characteristics of vegetation canopies with airborne radar measurements. *International Journal of Remote Sensing* 14:2803–2818.
- Resource Management Services. 2004. State of montana multi-hazard mitigation plan and statewide hazard assessment. Fort Harrison, MT: Department of Military Affairs, Disaster and Emergency Services.
- Shrivastava, H.S., P. Patel, Y. Sharma, and R.R. Navalgund. 2009. Large-area soil moisture estimation using multi-incidence-angle RADARSAT-1 SAR data. *IEEE Transactions on Geoscience and Remote Sensing* 47(8):2528–2535.
- Shrivastava, S.K., N. Yograjan, V. Jayaraman, P.P.N. Rao, and M.G. Chandrasekhar. 1997. On the relationship between ERS-1 SAR/backscatter and surface/sub-surface soil moisture variations in vertisols. *Acta Astronautica* 40(10):693–699.
- Shoshany, M., T. Svoray, P.J. Curran, G.M. Foody, and A. Perevolotsky. 2000. The relationship between ERS-2 SAR backscatter and soil moisture: Generalization from a humid to semi-arid transect. *International Journal of Remote Sensing* 21(11):2337–2343.
- Story, G. 2009. The difficulty of achieving good precipitation estimates for use in real-time drought monitoring. Sixth U.S. Drought Monitor Forum, Austin, TX, October 7–8.
- Svoboda, M.D., M.J. Hayes, and D.A. Wilhite. 2001. The role of integrated drought monitoring in drought mitigation planning. *Annals of Arid Zone* 40(1):1–11.
- Svoboda, M., D. LeComte, M. Hayes, R. Heim, K. Gleason, J. Angel, B. Rippey, R. Tinker, M. Palecki, D. Stooksbury, D. Miskus, and S. Stephens. 2002. The drought monitor. *Bulletin of the American Meteorological Society* 83(8):1181–1190.
- Takada, M., Y. Mishima, and S. Natsume. 2009. Estimation of soil surface properties in peatland using ALS/PALSAR. *Landscape and Ecological Engineering* 5(1):45–58.
- Teng, W.L., J.R. Wang, and P.C. Doriaswamy. 1993. Relationship between satellite microwave radiometric data, antecedent precipitation index, and regional soil moisture. *International Journal of Remote Sensing* 14:2483–2500.
- Texas Water Development Board. 2007. Highlights of the 2007 state water plan. *Water for Texas 2007*, Document No. GP-8-1.
- Tsai, W.-Y., S.V. Nghiem, J.N. Huddleston, M.W. Spencer, B.W. Stiles, and R.D. West. 2000. Polarimetric scatterometry: A promising technique for improving ocean surface wind measurements. *IEEE Transactions on Geoscience and Remote Sensing* 38:1903–1921.

- U.S. Census Bureau. 2005. County and county equivalent areas. http://www.census.gov/geo/www/cob/co_metadata.html (last accessed on December 15, 2011).
- USDA. 2009a. SCAN—soil climate analysis network. SCAN Brochure, Natural Resources Conservation Service, National Water and Climate Center National Soil Survey Center, Lincoln, NE. <http://www.wcc.nrcs.usda.gov/scan/SCAN-brochure.pdf> (last accessed on December 15, 2011).
- USDA. 2009b. SNOTEL and snow survey and water supply forecasting, SNOTEL Brochure, NWCC Rev3/09, Natural Resources Conservation Service, National Water and Climate Center (NWCC), Portland, OR. <http://www.wcc.nrcs.usda.gov/snotel/SNOTEL-brochure.pdf> (last accessed on December 15, 2011).
- Verdin, J., C. Funk, R. Klaver, and D. Roberts. 1999. Exploring the correlation between Southern Africa NDVI and Pacific sea surface temperatures: Results for the 1998 maize growing season. *International Journal of Remote Sensing* 20(10):2117–2124.
- Wagner, W., J. Noll, M. Borgeaud, and H. Rott. 1999. Monitoring soil moisture over the Canadian prairies with the ERS scatterometer. *IEEE Transactions on Geoscience and Remote Sensing* 37(1):206–216.
- Wagner, W. and K. Scipal. 2000. Large-scale soil moisture mapping in western Africa using the ERS scatterometer. *IEEE Transactions on Geoscience and Remote Sensing* 38(4, Part 2): 1777–1782.
- Wang, J.R. 1983. Passive microwave sensing of soil moisture content: The effects of soil bulk density and surface roughness. *Remote Sensing of Environment* 13:329–344.
- Wang, J.R. 1985. Effect of vegetation on soil moisture sensing observed from orbiting microwave radiometers. *Remote Sensing of Environment* 17:141–151.
- Wang, J.R. and B.J. Choudhury. 1981. Remote sensing of soil moisture content over bare field at 1.4 GHz frequency. *Journal of Geophysical Research* 86:5277–5282.
- Western Governors' Association. 2004. *Creating a Drought Early Warning System for the 21st Century, The National Integrated Drought Information System*. Denver, CO: Western Governors' Association. <http://www.westgov.org/wga/publicat/nidis.pdf> (last accessed on December 15, 2011).
- Wigneron, J.-P., L. Laguerre, and Y.H. Kerr. 2001. A simple parameterization of the L-band microwave emission from rough agricultural soils. *IEEE Transactions on Geoscience and Remote Sensing* 39:1697–1707.
- Wilhite, D.A. and M.H. Glantz. 1985. Understanding the drought phenomenon: The role of definitions. *Water International* 10:111–120.
- WMO (World Meteorological Organization). 2009. Experts agree on a universal drought index to cope with climate risks. Press release, World Meteorological Organization, WMO No.-872, United Nations, Geneva, Switzerland. http://www.wmo.int/pages/mediacentre/press_releases/pr_872_en.html (last accessed on December 15, 2011).
- Zhang, X.Y., M. Goldberg, D. Tarpley, M.A. Friedl, J. Morisette, F. Kogan, and Y.Y. Yu. 2010. Drought-induced vegetation stress in southwestern North America. *Environment Research Letters* 5(2):024008, doi:10.1088/1748-9326/5/2/024008.

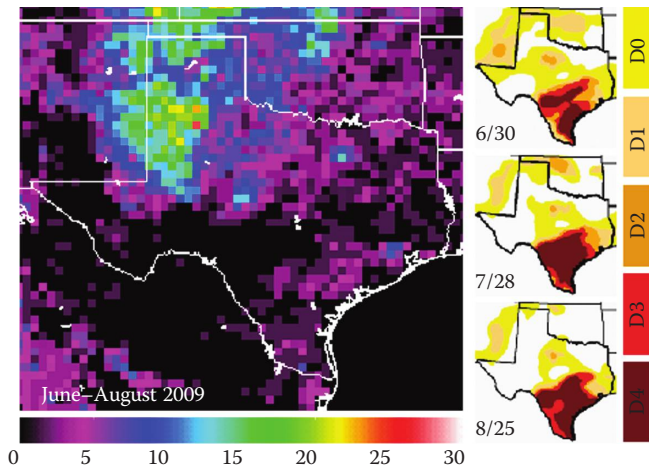


FIGURE 9.4 Effective precipitation frequency (%) measured by QSCAT for the period June–August 2009 (left panel) and drought levels from D0–D4 from the USDM for weeks ending on the marked dates in 2009 (right panels). The USDM drought levels include D0 for abnormally dry, D1 for moderate drought, D2 for severe drought, D3 for extreme drought, and D4 for exceptional drought. (Ref. Svoboda et al. 2002.)

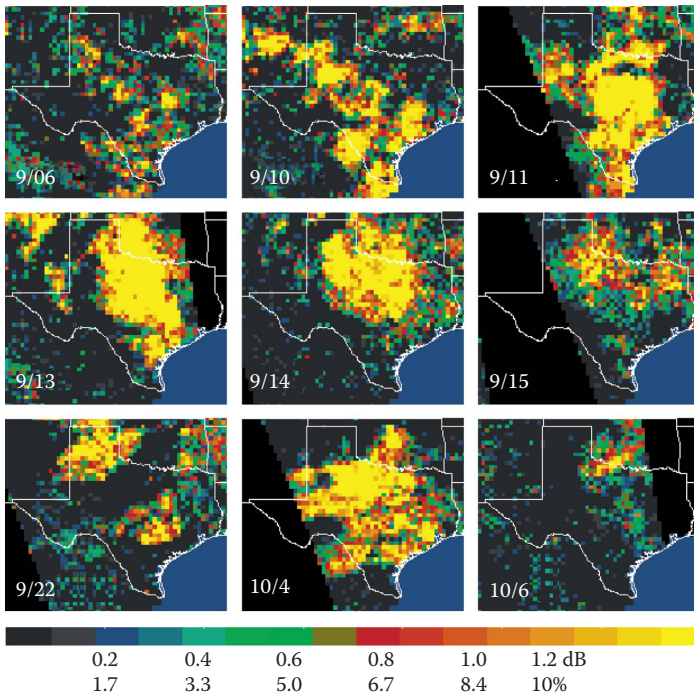


FIGURE 9.5 SMC measured by QSCAT with the vertical polarization along ascending orbits in September to early October 2009. The color scale represents backscatter change in dB and volumetric SMC in % with the Lonoke rating.

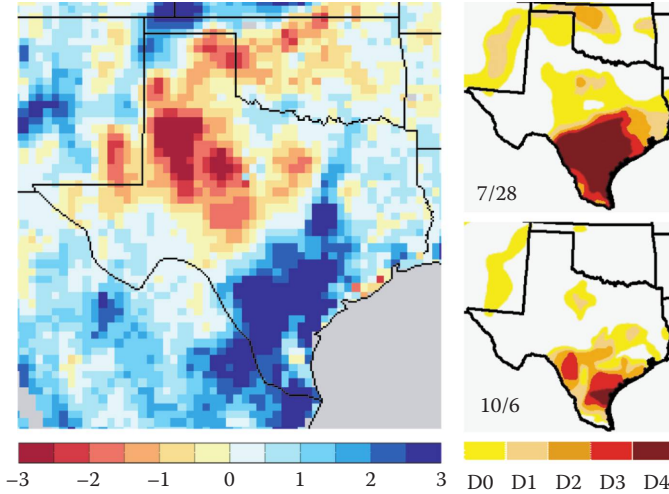


FIGURE 9.6 Difference of AMSR-E monthly averaged soil moisture in % of m_v (September 7 to October 6, 2009) and m_v (June 29 to July 28, 2009) showing seasonal SMC (left panel), and drought condition change between USDA drought maps in July and in September 2009 (right panels).

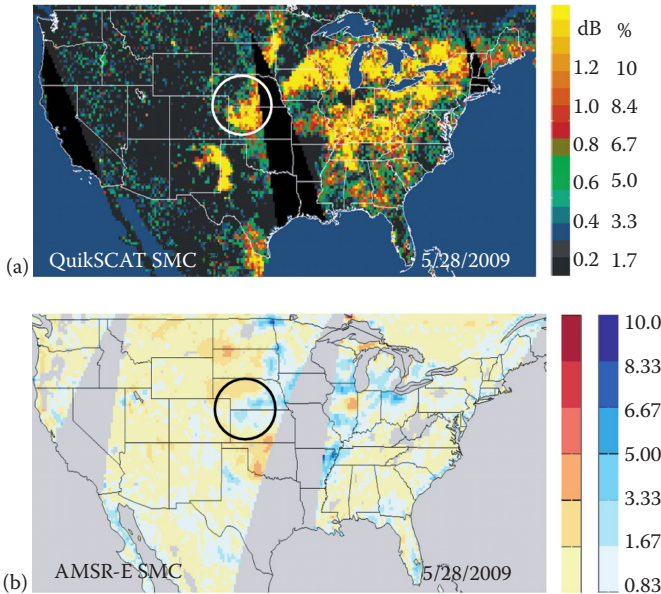


FIGURE 9.7 SMC on May 28, 2009, compared to the 2-week average between May 14 and 28, 2009, observed by (a) QSCAT SMC represented by backscatter change in dB and by volumetric moisture change in % from the Lonoke rating, and (b) AMSR-E by volumetric moisture change in % with yellow brown for drier and cyan blue for wetter conditions. The SMC maps are compared with Stage-4 24h precipitation measurements (NMQ, 2009) at 12:00 UTC in inches for (c) May 28, 2009, and (d) and May 27, 2009.

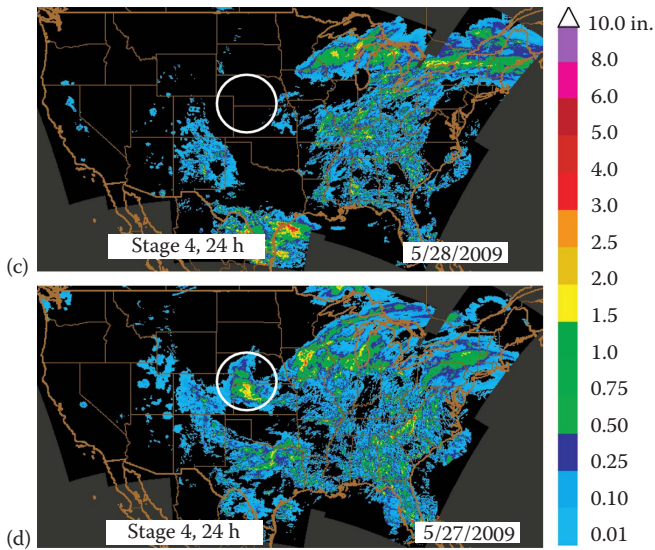


FIGURE 9.7 (continued)

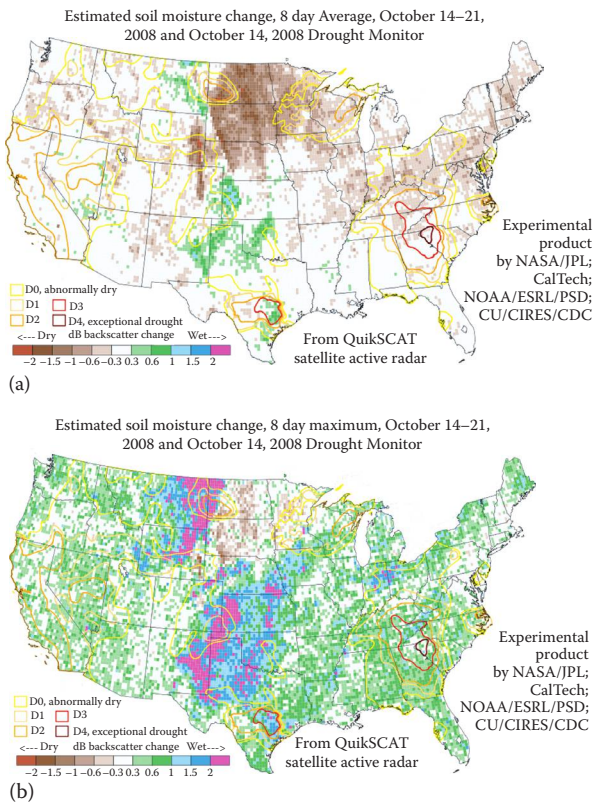
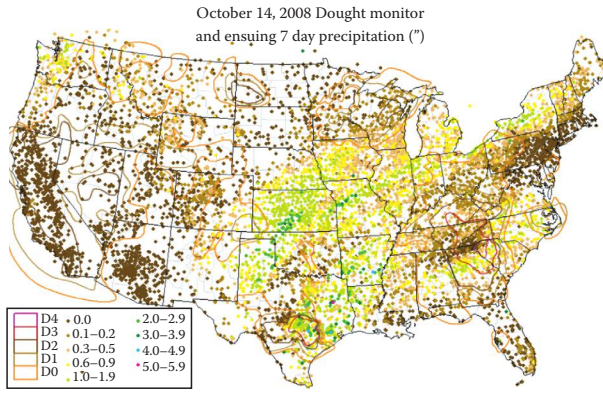


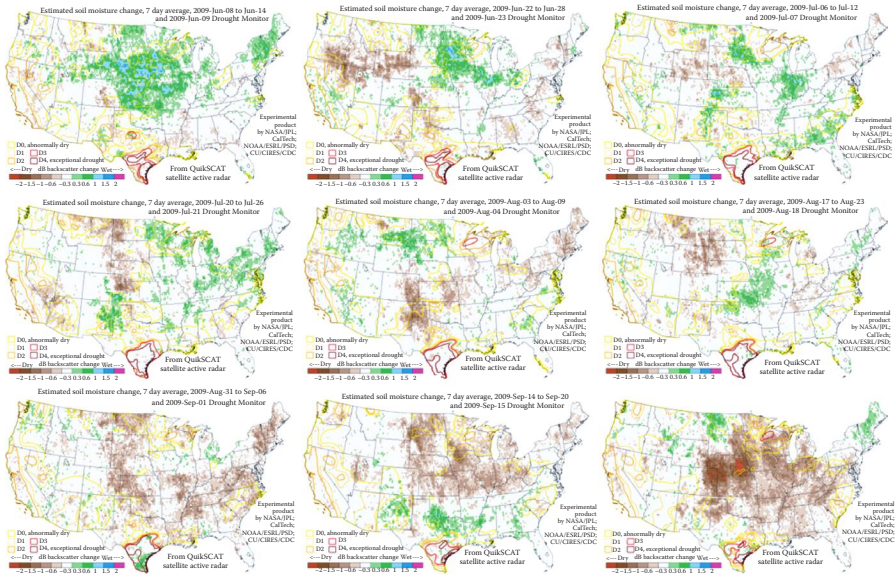
FIGURE 9.8 Comparison of QSCAT SMC with RGP for the period of October 14, 2008, and the ensuing 7 days: (a) mean SMC, (b) max SMC, and

(continued)



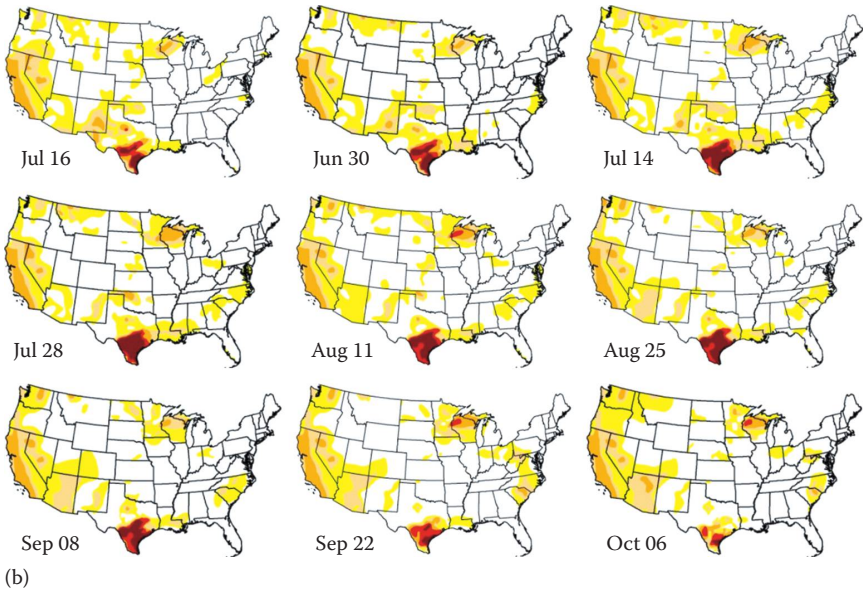
(c)

FIGURE 9.8 (continued) (c) RGP used in making USDM maps.



(a)

FIGURE 9.9 Weekly QSCAT mean SMC maps (a) and USDM maps (b) for the growing season in June–October 2009 (skipping a map once every other week).



(b)
FIGURE 9.9 (continued)